ABSTRACT

Title of Document: A NON-INTRUSIVE METHOD FOR TEMPERATURE MEASUREMENTS IN FLAMES PRODUCED BY MILLIGRAM-SIZED SOLID SAMPLES

Colleen Elizabeth Frances, Master of Science, 2014

Directed By: Dr. Stanislav Stoliarov, Assistant Professor, Department of Fire Protection Engineering

Fires are responsible for the loss of thousands of lives and billions of dollars in property damage each year in the United States. Flame retardants can assist in the prevention of fires through mechanisms which either prevent or greatly inhibit flame spread and development. In this study samples of both brominated and non-brominated polystyrene were tested in the Milligram-scale Flaming Calorimeter and images captured with two DSL-R cameras were analyzed to determine flame temperatures through use of a non-intrusive method. Based on the flame temperature measurement results, a better understanding of the gas phase mechanisms of flame retardants may result, as temperature is an important diagnostic in the study of fire and combustion. Measurements taken at 70% of the total flame height resulted in average maximum temperatures of about 1656 K for polystyrene and about 1614 K for brominated polystyrene, suggesting that the polymer flame retardant may reduce flame temperatures.

A NON-INTRUSIVE METHOD FOR TEMPERATURE MEASUREMENTS IN FLAMES PRODUCED BY MILLIGRAM-SIZED SOLID SAMPLES

By

Colleen Elizabeth Frances

Thesis submitted to the Faculty of the Graduate School of the
University of Maryland, College Park, in partial fulfillment
of the requirements for the degree of
Master of Science
2014

Advisory Committee:
Professor Stanislav I. Stoliarov, Ph.D., Chair
Professor Peter B. Sunderland, Ph.D.
Professor James A. Milke, Ph.D., P.E.

Dedication

To the people who have always seen my full potential, believed in all that I am capable of, loved me unconditionally and taught me the meaning of faith, mom and dad this one's for you. Thank you for being a living example of John 13:34.

Acknowledgements

There are several individuals and groups who have helped me to accomplish the work presented in this thesis, without whom I most certainly would not be where I am today. My sincere hope is that each of them truly understands how much they mean to me and how thankful I am for their dedication to my growth along this journey.

I would first and foremost like to extend my utmost gratitude to my advisor, Dr. Stas. His unparalleled dedication to not only furthering the scientific community but also the success and growth of his students is what made this thesis possible; I would not have been able to reach this milestone in my life without his help. Dr. Stas's knowledge and insight inspired me to challenge myself and to be persistent in all circumstances encountered during this project, and it was a pleasure to have him as my advisor. I am very thankful for the amount of time he has spent working with me and helping me to develop the professional skills I have acquired throughout the completion of this thesis.

I would like to also extend a tremendous amount of thanks to my colleague Fernando Raffan. Everyone knows Fernando as one of the supreme members of the "Council of Elders" in the Fire Protection Engineering Department, and it is no surprise why. He has dedicated an exceptional amount of time to assisting other students in our department, including myself, and is a tremendous asset to our department. Fernando, I hope you know how very much I appreciate all of your help. Without the countless MATLAB codes, experiments and data processing you have assisted me with along the way, I do not think I would have been able to complete this project. I have been blessed to work with you and call you a friend. I will always cherish this experience from the Hanami runs to our songs about lab life.

Haiqing Guo, thank you for setting the foundation upon which this research was built. I appreciate the time you invested into helping me understand the ratio pyrometry method and its governing physics and making yourself available whenever I had questions.

To my additional committee members, Dr. Sunderland and Dr. Milke, thank you for taking the time to be involved in my work and make this thesis the best it could be. I am thankful to have had the opportunity to have both of you as instructors as well as members of my committee, and appreciate your dedication to my success.

Thank you to Ajay Singh for providing me with the articles related to thermocouple measurements, they were tremendously helpful and informative. I very much appreciate your time and patience helping me to better understand the information presented in those papers.

I would also like to thank the supporting FPE staff including Olga Zeller, Sharon Hodgson, Mary Lou Holt, Nicole Hollywood and Pat Baker for their service. Each of them helped to keep my research moving in some way, and more often than not, their kind disposition and words of encouragement made many difficult moments pass easier.

Thank you to the members of my lab group for providing me with constructive criticism and assistance in and out of the laboratory. Specifically, thank you Xi for the work you did developing the MFC which I used in all my experiments. You all are an inspiration to me and motivate me to put as much heart into my work as you do.

Many thanks to the other FPE professors for the knowledge they have imparted on me as an undergraduate and graduate student. I thank them for making me the fire protection engineer I am today.

Thank you to BASF and the FAA for the funding and resources provided for this project. I would also like to thank the Fire Center for supplying the TA portion of my graduate assistantship, without both I may not have been able to purse my graduate studies.

To my family, Mom, Dad, Tom, Katie, Luke and Matthew, I love you more than you know. You are my rock and I am so blessed to have your unwavering love and support throughout every moment of my life. Thank you for believing in me and constantly encouraging me to chase my dreams.

Patrick, thank you for being there with a big 'ol hug and a shoulder to cry on any and every time I needed it. You believed in me even when it was difficult for me to do the same at times, and I can't thank you enough for being there every step of the way.

To my closest friends Ben and Rachel, thank you for all of the fun times and encouragement throughout the completion of my thesis. I can always count on the two of you to make me smile, and no matter what we will always be The Three Best Friends.

Last but by no means least, I would like to thank my Lord and Savior Jesus Christ for the countless blessings He has so richly provided to me, including the opportunity to pursue an advanced degree. May this work and my entire life bring praise and honor to Your Kingdom.

Table of Contents

List of Tables

List of Figures

List of Acronyms

FCC	Flaming Combustion Calorimeter
MFC	Milligram-scale Flaming Calorimeter
BFR	brominated flame retardant
PS	polystyrene
PSBr	brominated polystyrene
HRR	heat release rate
D-SLR	digital single-lens reflex
LOI	limiting oxygen index

1. Introduction

1.1 Brominated Flame Retardants

1.1.1 Uses and Benefits

Flame retardant materials with the capability of either slowing or eliminating fire growth are critical for engineering life safety through decreased material flammability. Flame retardant materials can be found almost everywhere and new materials are perpetually introduced to the market. In particular, a popular family of flame retardants is brominated flame retardants (BFRs). As with most flame retardants, BFRs have an array of uses including in textiles, electronics, and plastics (Alaee e. a., 2003), but of particular interest is the role of BFRs in aircrafts. To increase cabin safety, materials in commercial aircrafts must have flame retardant properties to minimize safety concerns if a cabin fire were to occur (Spengler, Allen, & McNeely, 2012). The presence of effective BFRs is particularly critical in aircrafts due to the difficulty or lack of evacuation means during flight as compared to a more typical building fire where evacuation is more straightforward.

BFRs are a specific type of polymer flame retardant containing the halogen bromine. Halogens are useful as additives in flame retardants because of their role in the combustion process. Combustion is a rapid oxidation process involving a fuel source and oxygen which generates heat or a combination of both light and heat. In particular, a thin reaction zone where chemical reactions propagate through an

unburnt fuel-air mixture is defined as a flame (Turns, 2012). For a hydrocarbon fuel denoted by C_xH_y, the stoichiometric combustion reaction is given by

$$C_xH_y + a(O_2 + 3.76N_2) \rightarrow xCO_2 + \left(\frac{y}{2}\right)H_2O + 3.76aN_2$$

Where $a=x+y/4$

It is commonly assumed that air composed of 21 percent oxygen and 79 percent nitrogen by volume serves as the oxidizer in combustion reactions, so the 3.76 preceding the nitrogen terms serves as an indication that for every mole of oxygen there are 3.76 moles of nitrogen.

The four primary steps of combustion are the preheating stage, volatilization or decomposition, combustion and propagation as illustrated by the following figure (Troitzch, 1990)

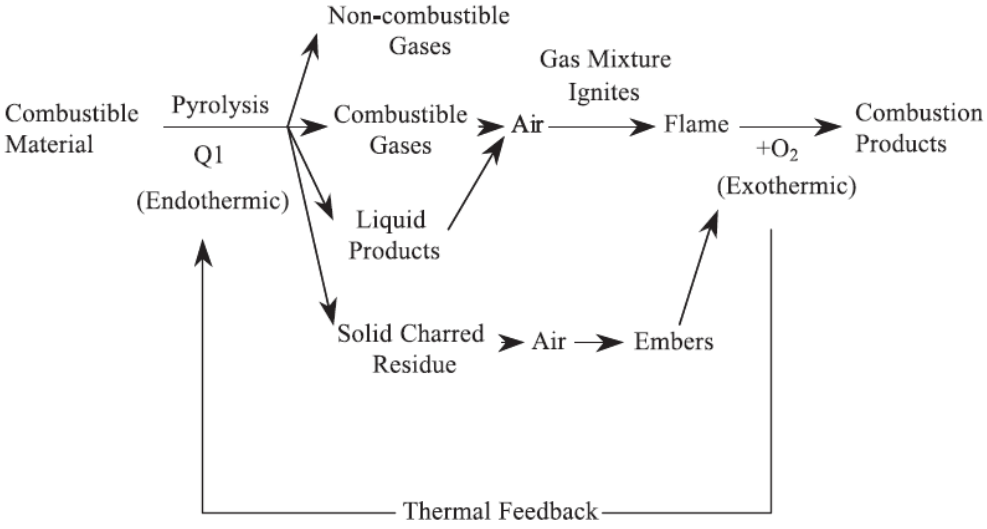

Figure 1-Illustration of the major steps of combustion

During the major steps of combustion, several intermediate series of chemical reactions occur, during which free radicals are produced. Halogens, which are highly reactive due to their chemical structure, capture free radicals produced during

combustion, the result being less oxidizing agents available and therefore less flame propagation. Bromine is a widely used halogen additive in flame retardants due to its size and radical trapping efficiency; bromine is one of the largest halogens which makes it effective at capturing radicals produced during combustion, while it also has a lower decomposition temperature compared to other halogens such as chlorine (Alaee e. a., 2003). It has been shown that when present in organic compounds, brominated and iodinated compounds are particularly effective flame inhibitors. Both halogens have high levels of recombination with reactive hydrogen radicals, which results in the formation of either HBr or HI. These species serve as scavenging agents, which are able to capture even more reactive radicals. Overall flame inhibition results from the decrease in the concentration of radicals which are highly reactive (Babushok, 1998) (Noto T. e., 1996) (Noto, Babushok, Hamins, & Tsang, 1998). In particular, for bromine, the competition of the following reactions is responsible for the destruction of hydrogen radicals where "RBr" is representative of the brominated compound (Babushok, 1998)

$H + RBr \rightarrow HBr + R$

$H + HBr \rightarrow H_2 + Br$

Additional formation of HBr and Br_2 is formed during recombination, thus more scavenging agents are available to actively trap radicals.

Although both brominated and iodinated compounds have been shown to inhibit radical formation and thus decrease flame propagation, brominated compounds are more practical for use in flame retardants. Iodine-containing compounds decompose at higher temperatures (Alaee e. a., 2003). This means that higher flame temperatures

would have to be present to prompt release of iodine in iodinated flame retardants, which is not ideal from a safety standpoint. BFRs, however, decompose at lower temperatures which means that flame inhibition is prompted earlier in the combustion process before higher temperatures are achieved. BFRs also compose the largest market group of flame retardants due to their low cost and combined high efficiency (Birnbaum & Staskal, 2004).

Like other polymer flame retardants, BFRs impede flame development in part through development of char. The presence of char correlates to thermal stability, because it limits mass and heat transfer during the burning process which results in a reduced heat release rate (HRR) and is representative of fuel being retained in the solid phase (Lyon & Janssens, 2005). Experiments conducted in the Milligram-scale Flaming Calorimeter (MFC), formerly the Flaming Combustion Calorimeter (FCC), which will be further discussed later, by Ding showed that for polystyrene (PS) samples, an increase in the amount of brominated PS by weight resulted in an increase in the amount of char (wt. %) coupled with a decrease in total HRR. Similar results were also apparent in Cone Calorimeter and Microscale Combustion Calorimeter test results (Ding, 2013).

1.1.2 Safety Issues and Alternatives

Several research efforts have concentrated on the harmful effects of BFRs including Tetrabromobisphenol A, polybrominated biphenyls (PBBs), Penta-, Octa-, Deca-brominated diphenyl ether (oxide) and hexabromocyclododecane. A review by Birnbaum (Birnbaum & Staskal, 2004) suggested that although existing data is limited, BFRs have the ability to accumulate in both animal and human tissues

depending on the severity and frequency of exposure, and PBBs specifically have not been produced since the early 1970s due to an incident in Michigan where they mixed with animal feed, poisoning several affected individuals (Birnbaum & Staskal, 2004). A review by Darnerud also presented that BFRs can accumulate in human breast milk and adipose tissues and may even be carcinogenic in high doses of exposure. On an acute level, BFRs also can result in irritation of mucous membranes as determined in rodent studies (Darnerud, 2003). This effect could be detrimental to human occupants if exposed to large amounts of BFRs in a building fire, as irritation of mucous membranes including the eyes can impair an individual's ability to exit a building safely and efficiently.

Due to the health and safety threats as well as corrosive properties posed by certain BFRs and other halogenated flame retardants, several alternative flame retardants are becoming widely used due to their lack of generation of harmful chemicals and gases during the combustion process. Flame retardants containing silicon are composed of additives which have less adverse effects on the environment. They also promote char formation in the condensed phase of combustion and trap active free radicals in the gas phase. In the same manner, boron-containing flame retardants promote formation of char in the condensed phase which redirects decomposition in favor of carbon instead of carbon monoxide (CO) or carbon dioxide (CO_2). Flame retardants containing phosphorus are also advantageous in place of BFRs due to their existence in various chemical oxidation states, making them versatile in a variety of material applications. Additionally, nitrogen-containing flame retardants are advantageous in certain applications because they are less toxic

and have a low evolution of smoke during combustion. Materials based on nitrogen-containing flame retardants may also be recycled, a positive effect for the environment (Lu & Hamerton, 2002).

The BFR used in this project was SAYTEX HP-3010, whose structure is shown below:

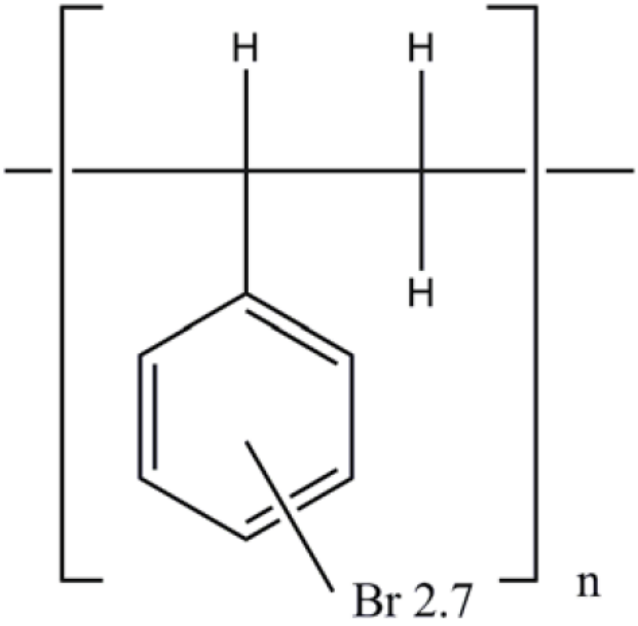

Figure 2-SAYTEX HP-3010 molecular structure

The "2.7" subscript on the bromine molecule merely indicates that certain aromatic groups in the polymer chain contain two bromine molecules while slightly more have three. The tested polymer is a non-blooming BFR and does not have reported concerns in the context of bioaccumulation (Albemarle Corporation, 2011). SAYTEX is also a large polymeric BFR which is entangled by intramolecular Van der Walls bonds, so it is not readily present in the environment like some other types of BFRs mentioned previously. Although several types of BFRs have been proven to have harmful effects to both humans and the environment, the polymer tested in the

context of this project has no such effects reported. The United States Environmental Protection Agency also has provided recent evidence that brominated polystyrene presents a low hazard in regards to human health effects, aquatic toxicity and bioaccumulation (EPA, 2014). The EPA also noted that risk of bioaccumulation of brominated polystyrene is low due to its large size and high molecular weight as mentioned previously in conjunction with the fact that it is not soluable in water.

1.2 Scope of Project

1.2.1 Existing Work

Temperature is an important parameter of flames but can be difficult to measure, especially in flames produced from solid fuels. In particular, laminar diffusion flames were of interest in this study. Two widely accepted methods of temperature measurement in such flames are both thermocouple measurements and ratio pyrometry. Flame temperature measurement through thermocouple use is a common practice in the context of combustion; however, thermocouples can be difficult to work with. Assembly is very tedious, especially with thermocouples with thin wires, and determining the proper heat transfer correlations is difficult when bead diameter and/or emissivity are unknown. An additional drawback of obtaining flame temperatures with thermocouples is that thermocouples only provide point measurements at specific heights and corresponding radii of a flame. The ratio pyrometry method; however, is a well-established method for determining flame temperatures non-intrusively without emissivity effects (Mollmann, 2011). The method is very spatially sensitive, but flame temperature measurements can be obtained without physically disrupting the flame as with thermocouples, and a

temperature profile at a height of interest may be obtained instead of a single point measurement. An approach to measuring flame temperatures of polymers was of particular interest in this project, so the ratio pyrometry method was used, with source signals coming from two different flame images obtained with digital single-lens reflex (D-SLR) cameras. The MFC, which was already developed was extended to include flame temperature measurements through a few alterations to the original set-up. Further details of this process will be discussed in subsequent sections.

The use of commercially available digital SLR cameras for the purpose of flame soot diagnostics has been studied and developed by several research professionals in the contexts of various flames and conditions. Sunderland and Faeth utilized a ratio pyrometry technique with the aid of a photomultiplier in laminar acetylene and hydrocarbon jet flames, but the method presented limitations in that traversing the optics across each height of the flames at a particular wavelength was required (Sunderland, Koylu, & Faeth, 1995) (Sunderland & Faeth, 1996). In a similar fashion, Gulder and colleagues utilized a ratio pyrometry method in laminar jet diffusion flames with the aid of a charged coupled device (CCD), but encountered similar limitations as Sunderland and Faeth (Snelling, 2002) (Joo & Gulder, 2009) (Mandatori & Gulder, 2011). Additional work by Faeth included ratio pyrometry soot diagnostic methods of microgravity flames with the aid of gray-scale CCD video cameras at visible and infrared wavelengths, but the cameras used did not have exceptional graphic properties, as they had low bit depth and pixel counts (Connelly, 2005). Long and colleagues; however, used a modern digital still camera and a three-color ratio pyrometry method without the aid of external bandpass filters in their

work (Kuhn, 2011), but their methods introduced greater uncertainties than those present in narrowband methods of a similar experimental design (Fu, Cheng, & Yang, 2008).

Furthermore, recent technique developments by Guo utilize a digital camera to obtain soot diagnostics that include temperature meaurements and soot volume fractions through a ratio pyrometry method with measurements taken at three wavelengths (Guo, Castillo, & Sunderland, 2013). The uncertainty of this non-intrusive method in the context of axisymetric jet flames is within 50 K of expected temperatures and is in close agreement with previous work (Santoro, 1987). The ratio pyrometry technique developed by Guo is the basis upon which this project's experimental techniques were developed and will be discussed in more elaborate detail later.

1.2.2 Research Motivation

Although there have been several developments in soot diagnostics through the use of digital cameras, a limitation of this work is that it has been confined to gaseous flames which have a steady supply and constant mass flow rate. Currently no work has been done which addresses the non-intrusive measurement of soot temperatures in flames of solid fuels. The objective of this project was to develop a non-intrusive technique which would allow for determination of polymer flame temperatures based on the methods utilized by Guo (Guo, Castillo, & Sunderland, 2013). It is already understood that BFRs reduce flame growth and development (Lyon & Janssens, 2005), but the mechanisms in which BFRs react in the gas phase of polymer burning is not well understood, and little to no research has been

conducted to address the subject (Linteris, 2011). This project was also motivated by the prospect of obtaining an important flame diagnostic, that is temperature, which can aid in a better understanding of how BFRs work in the gas phase, including changes that occur during the combustion process with respect to oxygen consumption and HRR. Results from tests performed by Ding (Ding, 2013) demonstrated that an increase in bromine content of polymer samples resulted in increased chair yield and decreased HRR, so it is hypothesized that an increase in the amount of bromine in a BFR sample will also result in a decrease in flame temperature.

1.3 Milligram-Scale Flaming Calorimeter

1.3.1 Development and Use

The Milligram-Scale Flaming Calorimeter (MFC), formally the Flaming Combustion Calorimeter (FCC) was recently developed by Ding at the University of Maryland (Ding, 2013). The primary motivation for developing and testing the MFC was to create an additional diagnostic for material flammability testing that was cost-effective in nature. Due to the harmful nature of certain BFRs, alternative flame retardant materials have been introduced to the market (Alaee & Wenning, 2002), and testing of these materials is imperative to determine their behavior in the context of combustion. Existing tests used previously to determine material flammability include limiting oxygen index (LOI), UL94, micro scale combustion calorimetry (MCC), smoke, flame spread and cone calorimeter tests.

LOI tests are used to determine the minimum concentration oxygen needed to prompt combustion for a sample in a nitrogen/oxygen mixture. Samples are

positioned vertically in an enclosed tube and subject to a small piloted ignition source as the oxygen concentration is gradually increased. A reported LOI value greater than 21% (vol./vol.) is indicative of a fire resistant material since oxygen is typically assumed to comprise 21% of air (SpecialChem, 2014) (University of Central Lancashire, 2014). An example of an LOI test set apparatus is shown in Figure 3

Figure 3-Limited Oxygen Index test apparatus

The UL94 test is a small-scale standard test for plastic materials' flammability and is characterized by either horizontal or vertical burn conditions. During vertical testing, samples are vertically positioned and subject to an ignition source at the bottom of the specimen. The ignition source is applied for ten seconds, removed until flaming no longer persists, and then the ignition source is reapplied for an additional ten seconds before removal. Two series of tests occur with five samples tested per series. The schematic illustration in Figure 4 depicts a vertical UL94 test (Underwriters Laboratories, 2014)

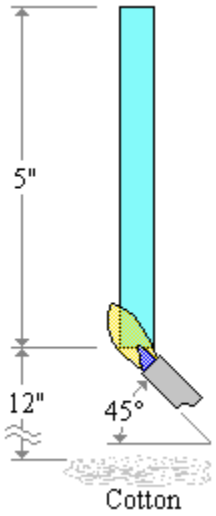

Figure 4-Illustraion of UL94 vertical test set-up

Based on the time for the samples to self-extinguish a rating of V2, V1 or V0 is assigned, with a rating of V0 having the most stringent requirements. Samples may also fall under the classification of 5VA or 5VB if they are subject to an ignition source that is more severe than the source used in tests where a rating of V2, V1 or V0 is obtained (Underwriters Laboratories, 2014).

The MCC apparatus was developed by the Federal Aviation Administration (FAA) and provides useful gas-phase diagnostics of polymer samples on the order of 5 mg (Lyon & Walters, 2002). The MCC relies on pyrolysis-combustion flow calorimetry to measure the rate of heat of combustion of fuel gases that are released by samples subject to a gas stream source. Products of combustion including carbon dioxide, water and acidic gases are removed from the gas stream by scrubbers in the MCC which allows for determination of the transient HRR through non-flaming combustion. An advantage of the MCC is that very small samples are required for each test.

The cone calorimeter is one of the most commonly used apparatuses for determining material HRR characteristics and is used to meet numerous existing Standards (Fire Testing Technology, 2014). The cone calorimeter is advanced in nature, and provides a wide breadth of data which can be used to determine the methods by which various material samples react to fire and a radiant heat source. Shown in Figure 5, the main components of the cone calorimeter include a conical heater, load cell with electronic tare, spark igniter, exhaust system, and various analysis systems (SINTEF, 2005).

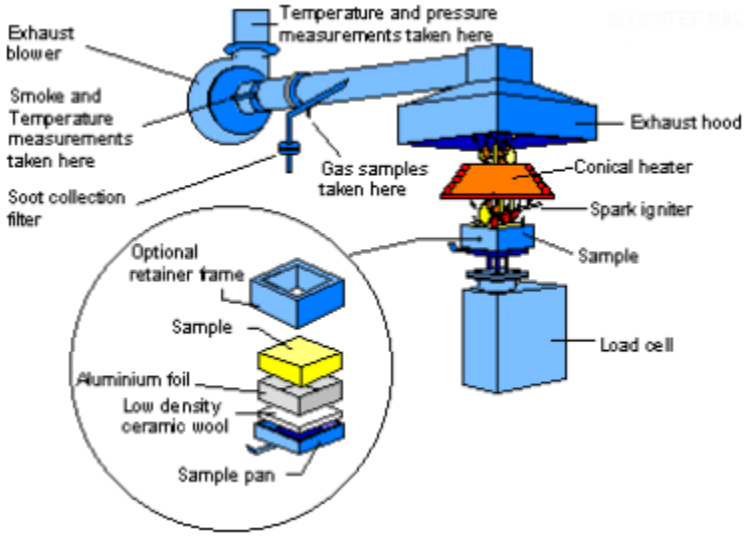

Figure 5-Schematic illustration of a cone calorimeter

The conical heater within the cone calorimeter provides a specified constant radiant heat flux to the flat 100 mm by 100 mm square sample which prompts the production of volatile gases. These gases are then ignited by a spark igniter which serves as a piloted ignition source. Gases produced from the flaming sample are collected through the gas sampling ducts. The gas sampling portion of the cone allows for analysis of several parameters including HRR, rate of smoke production, and carbon monoxide (CO) production. A laser system within the cone also allows for

determination of smoke obscuration through photodiodes. Additionally, the load cell of the cone is equipped with an electronic tare which has the ability to measure the mass of the sample as a function of time which is useful in determination of burning rate calculations.

Several of the existing test methods for material flammability are advantageous in that they have been thoroughly developed and are reputable in the combustion community. In particular, the cone calorimeter is perhaps the most widely used and recognized material testing HRR diagnostic available. Reliable test methods such as the cone calorimeter are vital to bridge the knowledge gap that currently exists in the field of gas phase combustion mechanisms. Very little is currently known about the specific ways materials combust in the gas phase (Linteris, 2011), so research efforts related to this field of study are of the utmost importance.

In the context of BFRs, several types of BFRs have been deemed harmful as they pose risks of bioaccumulation and may be carcinogenic in high doses (Darnerud, 2003). Related parties in the scientific community have sought alternative flame retardants that do not present adverse effects, but as new flame retardants are introduced to the market, these materials must be tested to determine their properties of chemistry and flammability. Material testing can be extensive in nature and require many samples, which can be expensive when larger samples are required. For this reason, the Milligram-scale Flaming Combustor (MFC), formally the Flaming Combustion Calorimeter (FCC), was developed to allow for a material flammability testing diagnostic that required much smaller samples than some of the traditional tests.

The MFC is a useful diagnostic tool, and as mentioned previously, can be used to determine material flammability properties in a cost-effective manner. The primary advantage of the MFC lies in the required mass of samples that are tested in it. MFC samples are typically finely ground powder or granulated polymers on the order of about 30 mg in mass which is vastly smaller than the more standard cone calorimeter samples which are on the order of about 50 g. Larger-sized samples required for cone calorimeter tests can be expensive; therefore, it is not cost-effective to test new materials in this device. The MFC is also advantageous for determining material properties and analyzing gas phase combustion mechanisms of new flame retardants, again because only a small sample size is required for each experimental run.

The primary diagnostic determined by the MFC is oxygen consumption, which is used to determine HRR as well as combustion efficiency. The project for which the MFC was developed aimed to determine comparative information about gas phase combustion properties of both pure and flame retardant-containing polymers, the hypothesized notion being that addition of flame retardants would result in a notable decrease in HRR, time to combustion and ignition time. The polymer sample flames can also be visually accessed in the MFC which allows for determination of additional combustion properties including combustion time and physical flame properties including height and overall shape.

The MFC is composed of four main parts which are shown in Figure 6:

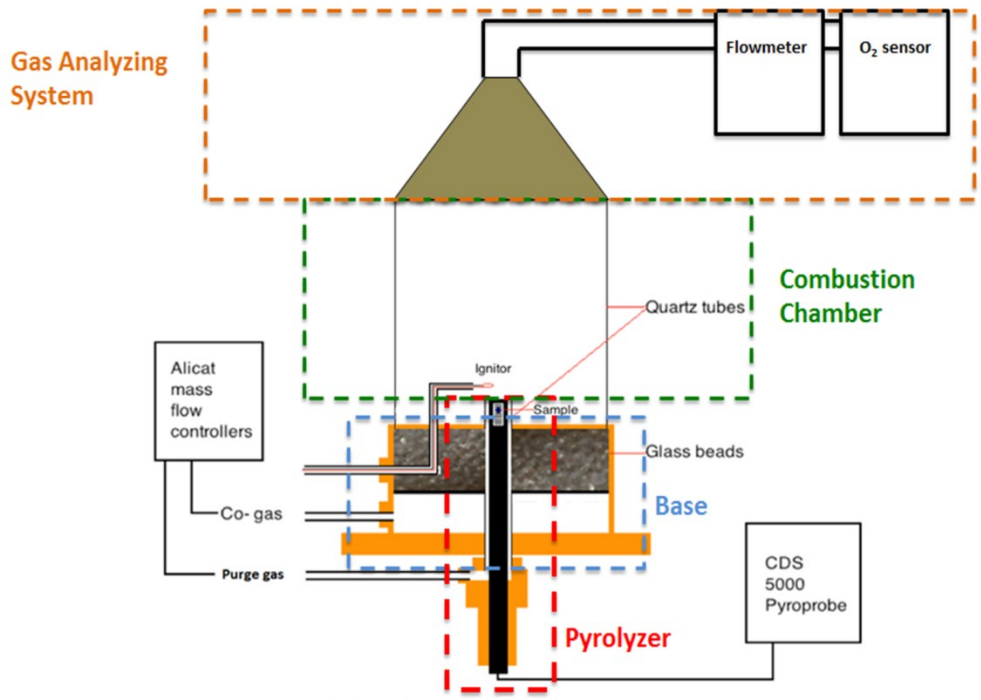

Figure 6-MFC schematic diagram

The pyrolyzer includes a long, narrow quartz tube which encloses the sample itself which is enveloped by a pyroprobe. The pyroprobe heats the sample at a constant heating rate ranging from 0.01°C/s to 999.9°C/s (a heating rate of 10°C/s was used in experiments), prompting combustion, while the igniter in the combustion chamber of the MFC acts as a piloted ignition source and produces a flame. The portion of the MFC serving as the base is used to supply co-flow and purge gases to burning samples and surrounds the narrow quartz tube containing the sample with glass beads to allow for the greatest homogeneity of surrounding gas to the sample as possible. The combustion chamber allows for a closed system with a larger cylindrical quartz tube around the base of the MFC which is connected to the gas analyzing system composed of a flow meter and oxygen sensor which allow for important diagnosis of aforementioned combustion properties. Data acquisition programs developed by Raffan and Ding using LabVIEW software were used to record electronic data from

the MFC tests that was used in laboratory data analysis. For more details regarding the MFC apparatus, the interested reader is directed to Ding's thesis (Ding, 2013).

1.3.2 Relevance to Project

The MFC was designed to allow for small-scale tests of polymer samples that can be used to determine combustion properties, providing insight on gas-phase mechanisms of BFRs, in particular the interaction of the chemical and physical processes in diffusion flames which are not well-understood. Temperature is an additional parameter which is commonly measured in a broad application of laboratory settings and is a main characteristic of the flame structure. The ability to measure polymer flame temperatures with the aid of the MFC is invaluable, as it is less expensive to produce milligram-scale samples and provides an additional gas phase diagnostic. The non-intrusive method of temperature measurement has also never been applied to solid fuels, so a large number of test runs were necessary to produce reliable results. This made the MFC especially useful for the application of this technique due to the fact that only about 30 mg of sample material per test run was necessary.

2. Experimental Procedures

2.1 Mathematical Basis

2.1.1 Planck's Law

After both cameras were calibrated spatially, the MFC was used to produce a flame, first with propane as the fuel source during validation stages, then with polymers. Signal intensities from flame images which were line-of-sight intensity distributions were then deconvoluted to obtain radially distributed intensities since flames were assumed to be axisymmetric. Based on Planck's Law, the intensity distributions could be translated to flame temperature profiles.

Planck's Law provides a relationship between spectral radiance and wavelength for a corresponding temperature. The formula for temperature on which data analysis was based is given by Formula (1)

$$W_\lambda = \frac{W\pi hc^2\varepsilon}{\lambda^5\left[\exp\left(\frac{hc}{\lambda kT}\right)-1\right]} \quad (1)$$

Where

W_λ is spectral radiance, in W/m^2

h is Planck's constant, 6.626e-34 m^2 kg/s

c is the speed of light, 3e8 m/s

ε is emissivity, which is 1 for a blackbody

λ is wavelength

k is Boltzmann's constant, 1.380e-23 m^2 kg/s^2 K

T is temperature, in Kelvin

(Planck, 1901)

This mathematical relationship can be modified for the ratio pyrometry application which was used to determine soot temperature profiles for the examined flames at specific heights of interest. The modified formula is dependent on information obtained from two different cameras, each with a corresponding wavelength that was associated with the specific camera.

2.1.2 Ratio Pyrometry

As previously mentioned, a ratio pyrometry method similar to that utilized by Guo and colleagues was utilized in this project. The method is dependent on intensity values that are obtained from each of two digital cameras as photos of the flame of interest are simultaneously captured by the two cameras. The formula used to calculate temperature values based on the cameras' outputs is determined by taking the ratio of the Planck's Law formula for two signal intensities obtained from two cameras, each with an associated wavelength of interest. Through algebraic means, the temperature as a function of signal intensity may be determined and is given in Formula (2)

$$T = \frac{\frac{hc}{k}\left(\frac{1}{\lambda_2} - \frac{1}{\lambda_1}\right)}{\ln\left[\frac{S_{\lambda_1}}{S_{\lambda_2}}\frac{C_2}{C_1}\left(\frac{\lambda_1}{\lambda_2}\right)^{a}\right]} \tag{2}$$

Where

T is temperature, in Kelvin

h is Planck's constant, 6.626e-34 m^2 kg/s

c is the speed of light, 3e8 m/s

k is Boltzmann's constant, 1.380e-23 m^2 kg/s^2 K

λ_1 is the first wavelength of interest, in meters

λ_2 is the second of the two wavelengths of interest, in meters

$S_{\lambda 1}$ is the normalized grayscale intensity reading from the camera associated with the first wavelengths of interest, in units of s^{-1}

$S_{\lambda 2}$ is the normalized grayscale intensity reading from the camera associated with the second wavelength of interest, in units of s^{-1}

C_2/C_1 is the calibration constant (Guo, Castillo, & Sunderland, 2013)

a is the correction factor for soot

The procedure for obtaining the calibration constant is further discussed in the subsequent section. Also it is notable that a, the soot correction factor is related to the emissivity of soot and wavelength. This value ranges from about 0.9 to 1.38, so a value of 1 was used in soot temperature calculations since it is roughly an intermediate value of the aforementioned range. The temperature profiles were not very sensitive to the value of the soot correction factor, with differences in maximum temperature values being 100 K between the minimum and maximum values of the soot factor.

In order for the ratio pyrometry method to yield the most accurate temperature profiles possible, two digital cameras were utilized to capture simultaneous images of a single flame in space and time, and each camera captured images at a specific

wavelength of interest. Specific details on experimental technique are further discussed in a subsequent section.

2.2 Calibration

2.2.1 Relation to Temperature Calculations

Calibration of both digital cameras was necessary to accurately translate each camera's intensity output values into temperature data. Individual cameras behave differently; therefore, it was vital to obtain the proper constant of calibration used in the modified Planck's Law equation. The calibration constant appears in the equation used to determine temperature as C_2/C_1 and it accounts for each camera's response to changes in temperature in relation to the wavelength associated with that specific camera. The calibration constant, however, is specific to pre-determined camera settings including distance from experiment, ISO, aperture, and white balance sensitivity, so any changes to these settings require that the user perform a new calibration based on revised conditions.

2.2.2 Procedure

Calibration was performed using an Oriel black body furnace (model 67032) with a cavity emissivity of 0.99 ±0.01%. The cameras used in both calibration and experiments were Nikon D800 digital SLR cameras with 36.3 mega pixels and a 14 bit depth per each of the three major color channels (R, G and B). The cameras' sensors were modified through a third party, Max Max LDP, LLC which extended the spectrum of wavelengths the cameras could detect, allowing images at infrared wavelengths to be captured. Camera modification by the third party was achieved by

removing a stock layer of glass contained in each camera and replacing it with the company's custom glass. Each of the two Nikon D800 cameras used was assigned to a particular wavelength of interest which corresponded to the central wavelength of a bandpass filter associated with that camera. The filters were both Andover Corporation circular bandpass filters 50 mm in diameter with a bandwidth of 10 +/- 2 nm. The first filter's center wavelength was 650 nm, and second filter's was 900 nm (part numbers 650FS10-50 and 900FS10-50, respectively). Each filter was mounted to a threaded filter holder 50 mm in diameter which allowed the filters to be directly attached to the lenses of their respective cameras. Each digital camera was equipped with a Nikon Nikkor 50 mm f/1.8D lens (product 2137) and a Nikon PK-12 14 mm Extension Tube (product 2652), which allowed for the best image focus. In experiments, each camera was 14.5 cm (145 mm) away from the center of the FCC burner, so during calibration, the cameras were also positioned 14.5 cm away from the cavity of the blackbody furnace and centered on the furnace cavity opening. Camera settings were also identical to those chosen for experimental runs which included an ISO value of 200, aperture of f/5 for an 11 mm depth of field, and white balance option of direct sunlight.

During the calibration itself, grayscale intensity data was captured by recording images of the blackbody furnace cavity at 900 °C up to 1200 °C in increments of 50 °C for each camera, since one camera was associated with the 650 nm bandpass filter and the other camera was associated with the 900 nm bandpass filter. Shutter time was optimized for each camera at each temperature setting so that intensities were strong, yet not strong enough to saturate any of the color channels of

the cameras. Shutter times ranged from 1.6-1/25 s for the 650 nm camera and 1/3-1/50 s for the 900 nm camera. Once an optimal shutter time was determined at each temperature, four photos were captured for each camera.

After photos were captured by both cameras at each temperature, for a given camera a specific pixel location was selected as the position where image intensity data was extracted. The reported four intensities for each temperature data set for each wavelength were averaged to obtain "net" intensities, and these values were normalized by dividing the intensities by their respective shutter times at that temperature for each individual camera.

Since the emission source during calibration was a blackbody rather than soot, the emissivity of the source was known to be very close to 1, so the equation used to obtain temperature was modified to obtain the expression for the calibration constant in Formula (3)

$$\frac{C_2}{C_1} = \frac{\exp[\frac{\frac{hc}{k}\left(\frac{1}{\lambda_2}-\frac{1}{\lambda_1}\right)}{T}]}{\frac{S_{\lambda_1}}{S_{\lambda_2}}} \tag{3}$$

The $(\lambda_1/\lambda_2)^a$ term does not appear in the calibration constant equation since it serves as a corrective term for the emissivity of soot, so in the case of a black body with emissivity of 1, this term is not applicable. The mathematics suggest slight differences in calibration constant values between temperatures, so a slightly different constant value is obtained at each temperature of the blackbody furnace, which accounts for small uncertainties in the data. A "net" constant is therefore determined by averaging each of the seven individual calibration constants obtained from the

seven temperature settings at which intensity information is acquired. A MATLAB code was utilized to process images and obtain the calibration constant in an automated fashion.

Upon attainment of the calibration constant, an additional MATLAB code was used to check the accuracy of the constant. Using the original temperature equation with the known calibration constant, the normalized "net" intensities of each camera at each of the blackbody temperatures were used for the values of $S_{\lambda 1}/S_{\lambda 2}$. This would result in a theoretical temperature for comparison to the reported blackbody temperature used at each point of calibration (for example, it would be expected that for the images captured at 950 °C, the calculated experimental temperature would be very close to 950 °C as well). Validation of the calibration constant yielded favorable results, with values that were within about 20 K or less of the expected value, which corresponded to a percent difference of 3% or less. The obtained calibration constants varied slightly between experiments, as shown in Table 1 which provides a description of the experimental timeline

Table 1-Dates of Experiments and Calibrations

Date	Experiment	Result (if applicable)
5/14/2014	Propane	N/A
5/28/2014	Calibration	0.0586
6/4/2014	Calibration	0.0590
6/16/2014	PS and PSBr	N/A
6/24/2014	PS, PSBr and Propane	Increased camera exposure time for propane images

6/25/2014	Calibration	0.0652
7/1/2014	Propane	N/A
7/7/2014	PS and PSBr	N/A
7/8/2014	Calibration	0.0630

When temperature profiles were calculated, the calibration constant used was the once which was determined closest to the time of the experiment. For example, for the polymer test on 7/7/2014, 0.0630 was used as the calibration constant value in the formula for temperature. The exception was the calibration constant used to calculate flame temperature profiles from the 6/16/2014 polymer experiments. Since two calibrations were performed almost equally in time before and after the experiment, and average of the calibration constants obtained on 6/4/2014 and 6/25/2014 was used.

2.3 Technique Validation

2.3.1 Experimental Design

To ensure that flame soot images were captured identically in time and space of the same flame, the two Nikon D800 cameras were mounted 45 degrees offset of each other and centered relative to the MFC burner center. The aid of a laboratory breadboard and dove tail rail mounts allowed for the most precise set-up possible. Each camera was also mounted at the same height with an optical rail mount and was 14.5 cm away from the center of the MFC burner to allow for optimal field of view.

To reduce the possibility of flame flickering during experiments, a cage-like enclosure which surrounded the MFC was built from 80/20 equipment and had flame-retardant fabric attached to it to keep air from disturbing the flames during experiments. A square panel of PVC material was also placed on top of the "cage" frame to further block any unwanted air. This panel was immediately removed at the conclusion of polymer experiments so that soot particles and gases could properly ventilate and clear the experimental enclosure. An overhead view of the MFC and cameras set-up is shown in Figure 7.

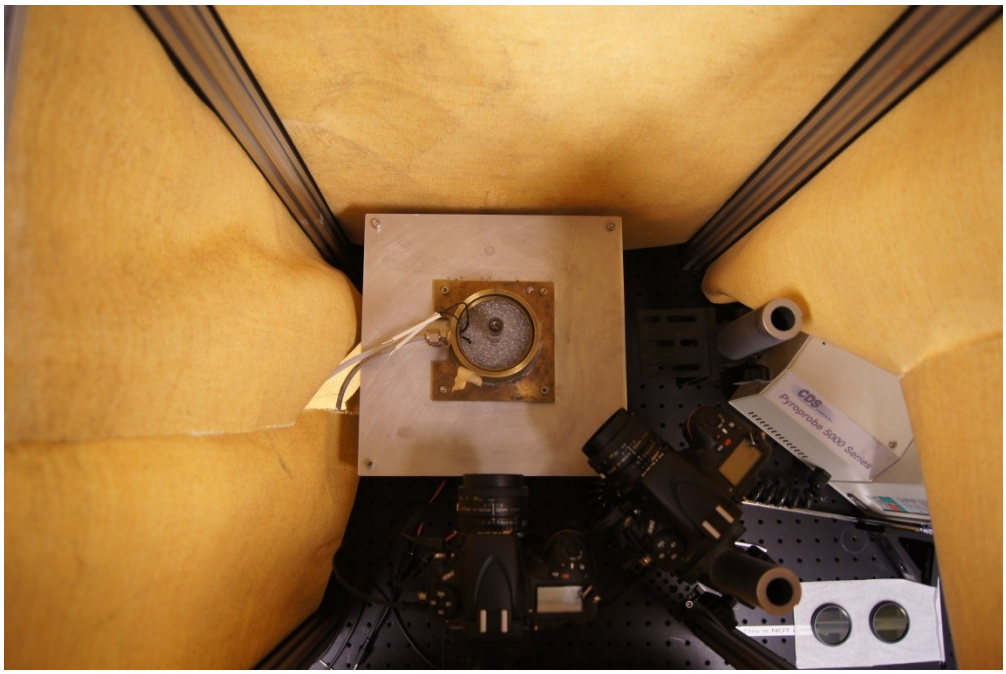

Figure 7-Overhead view of experimental set-up

To ensure that both cameras were properly positioned with respect to each other and the MFC, the calibration piece shown in Figure 8 was created with a 3D printer.

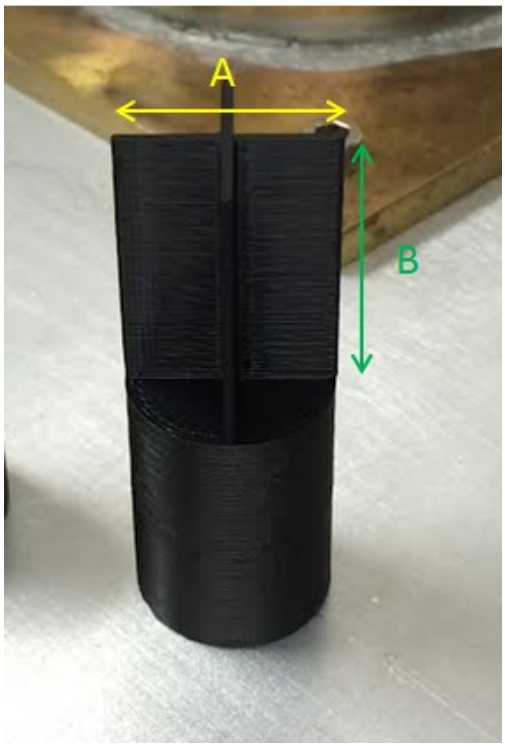

Figure 8-Camera calibration piece-dimension "A" was about 1600 pixels in length while dimension "B" was about 2200 pixels/1 in.

The calibration piece was designed to fit snugly on top of the MFC burner and was made of two intersecting planes perpendicular to each other so that the cameras could both be properly focused and positioned 45 degrees offset of each other. Positioning the cameras 45 degrees apart from each other was advantageous because it provided an indication of whether or not the flame was symmetric in both planes after images were captured. An additional advantage of the calibration piece was that it allowed for proper scaling when post-processing images. Photos of the calibration piece captured by each camera were analyzed using Spotlight 16 (Klimek & Wright, 2004) imaging software's line profile tool. A line was drawn across a known dimension of the calibration piece, and the line profile tool in Spotlight indicated how many pixels were included in the dimension of the piece which allowed for obtainment of the

proper pixel-to-millimeter conversion necessary to determine flame dimensions based on acquired images.

Similar methodology was used when positioning the cameras to ensure that both cameras had the same field of view. Images of the calibration piece were captured as both the 650 and 900 nm cameras were adjusted until the line length of the calibration piece dimension was within 10-15 pixels difference between the two cameras with the calibration piece rotated to face each camera when pictures of the piece were taken. The cameras were also positioned in such a way that the pixel numbers of a designated point in the calibration piece were within 10-15 pixels difference between the two cameras, which ensured that the cameras were properly aligned in space with respect to the MFC burner. This process allowed for determination of the length scale for each camera before each test based on photos of the calibration piece which was consistently about 86 pixels per millimeter.

After both cameras were positioned 45 degrees offset of each other in space, sample tests were run and images were obtained. Since the ratio pyrometry method relies on two images of a single flame, it was imperative to capture flame images at identical points in time. To do so, a Triggertrap TC-DC0 connector and mobile dongle were attached to each camera. The two Triggertrap devices were connected to a single Y splitter which was then injected into the headphone jack of a smart phone (in this case an Apple iPhone). A free app was downloaded to the mobile device, and upon triggering allowed flame images to be captured at identical points in time. The photos below were taken by two different cameras with the aid of Triggertrap in "slow" mode, capturing one image every second, while a stopwatch ran for several

seconds. Based on the photos in Figure 9 of the stopwatch captured by both the 650 (left) and 900 (right) nm cameras, it was apparent that each camera captured photos of the stopwatch at identical moments in time since both cameras recorded images of a stopwatch at 10.0 and 12.0 s; therefore, the Triggertrap proved to be an optimal tool for acquiring images of the same flame to be used for ratio pyrometry.

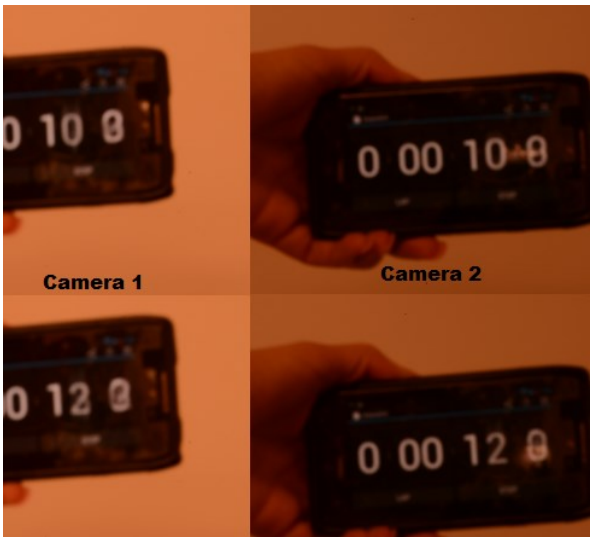

Figure 9-Stopwatch images captured with Triggertrap

Images from experiments were recorded in Nikon Electronic Format (NEF) or RAW format. To avoid gamma corrections, images were converted to TIFF format corresponding to images with three color planes (R, G and B) using the program dcraw created by D. Coffin. Dcraw commands "-4 –T –o 0" (Coffin) were entered in the computer dos window to properly convert images to the desired format. The folder which the dcraw commands were sent to contained the images being converted to TIFF format as well as the dcraw application file. Converted images were then analyzed in Spotlight to determine the signal intensity information necessary to determine flame temperature profiles.

The Abel Transform Tool in Spotlight was used to extract intensity profiles from the images of interest. The Abel transform is a mathematical integral transform used to convert line-of-sight projections to radial projects. Figure 10 illustrates the difference between the observed line-of-sight intensity distribution compared to the actual projection of the circular system, in this case the axisymmetric flame.

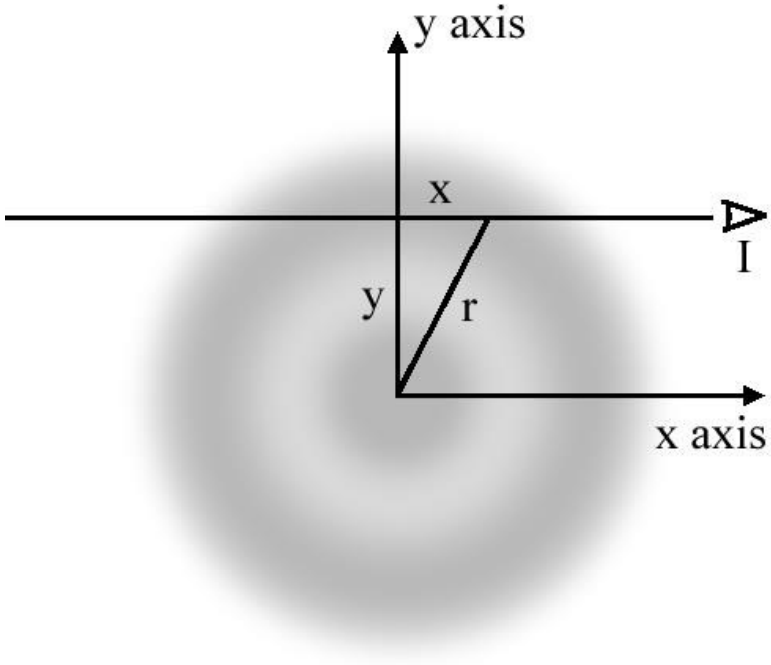

Figure 10-Illustration of intensity distributions with I being the observed line-of-sight distribution of the symmetric distribution shown in gray

The relationship between *p(l)*, the observed line-of-sight projection and *f(r)*, the radial distribution of interest is

$$p(l) = 2\int_{l}^{\infty} \frac{rf(r)}{\sqrt{r^2 - l^2}} dr \tag{4}$$

The Abel transform, which is an analytical inverse of the previous equation, is given by

$$f(r) = -\frac{1}{\pi}\int_{r}^{\infty} \frac{p'(l)}{\sqrt{l^2 - r^2}} dl \tag{5}$$

The Abel transform is advantageous in the application of line-of-sight to axisymmetric spatial distribution conversions, because it is an exact solution to the equation for *p(l)*, the line-of-sight projections and is more accurate than other mathematical methods which can be used for similar purposes (Yuan, 2003). In the context of ratio pyrometry, the Abel Transform Tool available in Spotlight was necessary to convert the line-of-sight intensity projections apparent in acquired images into radially distributed intensity profiles since flames were assumed to be axisymmetric. The deconvoluted intensity profiles acquired in Spotlight were then inserted into the temperature formula derived from Planck's law to obtain flame temperature profiles at a height of interest. Since the pixel-to-millimeter spacing determined from spatial calibration was slightly different between the two cameras, the MATLAB code used to generate plots of the temperature profiles at each height of interest adjusted for the two intensity profiles (one from the 650 nm camera and one from the 900 nm camera) so that they were scaled the same in millimeter space.

3. Propane Tests

3.1 Overview and Image Analysis

In order to successfully adopt the ratio pyrometry method for soot temperature measurements obtained from the MFC, propane was first used as the fuel source since it had a constant fuel supply and was relatively simple to work with. Since propane is a gaseous fuel, it has a near constant flow rate and no associated mass loss rate, which results in a flame that is virtually identical at various points in time. The general experimental set-up was the same in the propane tests as it was during the PS tests.

During preliminary tests, propane was supplied at a flow rate of about 50 standard cubic centimeters per minute (SCCM) while air was supplied as the co-flow gas at a flow rate of about 5 standard liters per minute (SLPM). Proper alignment of the two cameras was performed with the aid of the calibration piece as mentioned previously, and optimal shutter times were determined for each camera as to avoid oversaturating any of the three color channels in the camera. Additionally, both cameras were spatially calibrated before each test. The cameras were operated in "slow" mode at shutter times that resulted in image intensities that were about 50 to 75 percent of the maximum intensity before oversaturation occurred. The Triggertrap devices were used to trigger both cameras at identical points in time to ensure that image pairs of identical flames were captured. Although the propane flames were fairly steady and assumed to be axisymmetric, at times the flame would flicker due to laboratory conditions such as draft or movement of individuals in the lab. In these cases, a slower shutter time resulted in a longer camera exposure time which correlated to a faded image or one in which a double flame appeared to be present,

but a faster shutter time on the order of 1/10 of a second tended to eliminate this issue and captured a more instantaneous image of the flame. For the propane tests, shutter times between 1/10 and 1/20 s were used.

After multiple images were acquired, a series of analyses were conducted to determine which image pairs were suitable for data extraction for determination of flame temperature profiles. The diagram in Figure 11 provides a visual overview of each step.

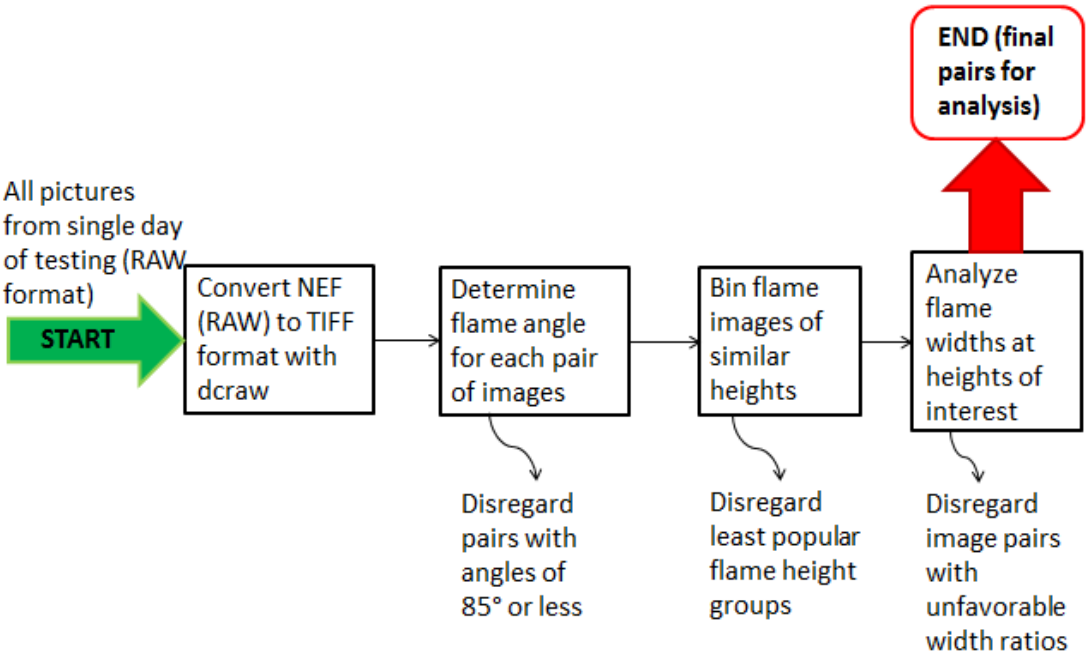

Figure 11-Block diagram of steps used to determine best flame image pairs for data analysis

After images were captured and converted to TIFF format as to avoid gamma corrections, a MATLAB code which analyzed the symmetry of each flame with respect to the center of the MFC burner was used to the determine which pairs of images were the most symmetric. The code determined the angle formed between the tip of the flame and the horizontal plane of the base of the burner in each acquired image. A pair of images captured with the 650 and 900 nm bandpass filters that both

had a reported flame angle close to 90° was indicative of a symmetric image pair of the same flame. An additional MATLAB code was used to determine the flame height of each image as well as the group of images that represented the most popular flame heights. The flame heights were determined from a MATLAB code which analyzed an intensity line profile along the centerline of the flame which was estimated as x-pixel coordinate of the burner centerline. Figure 12 provides a visual depiction of where several important points are on an example propane flame. The centerline of the flame was very close to the centerline of the MFC burner in the case of a symmetric flame.

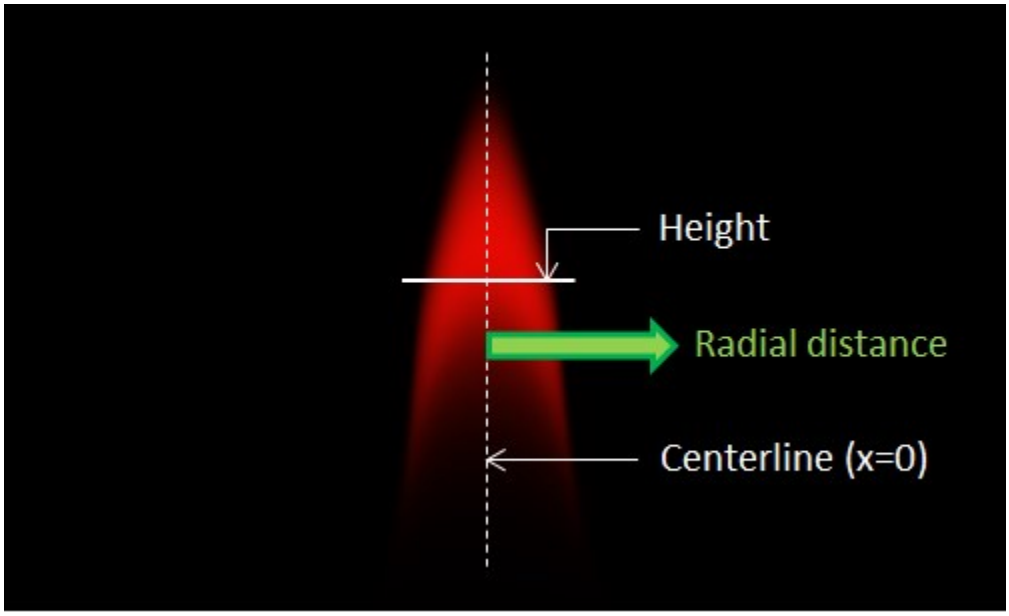

Figure 12-Visual of important locations on example propane flame

Based on image analysis, the y-pixel location on the flame image where the intensity was 10% of the maximum intensity was considered the tip of the flame. 10% of the maximum intensity of the flame was determined as the cutoff for the flame height due to previous inspection of flame images. The pixels on flame images with an intensity value of about 10% of the maximum were located close to the tip of the flame;

therefore, this was used for the criteria for flame height cutoff. The 900 nm flame images were consistently taller than the 650 nm flame images, so the absolute height in millimeter space at which temperature profiles were extracted were based on 650 nm images' total flame heights, and the corresponding 900 nm flame images' heights of interest were determined at an identical point in millimeter space. For example, if 54% of a 650 nm flame image's total height was 15 mm, intensity data for the corresponding 900 nm flame image was analyzed at 15 mm as well since 54% of the taller 900 nm image would not be at the same absolute location of the flame.

Propane flame images of similar heights were determined using a MATLAB code which performed a "sliding bin" analysis on the flame heights. A window of a set width was prescribed to the MATLAB code, in the case of propane flame images, 0.5 mm, and the MATLAB code reported how many flame images of a set height fell within the set window of flame heights. The "bin" which had a set width of 0.5 mm then shifted up by one third of the window width to analyze the amount of flame images that fell in the subsequent ranges of window values. For example, if the minimum flame height was 13 mm, the code would analyze a window from 13-13.5 mm and see how many flame images fell within that range of heights. The "bin" of set 0.5 mm width would then slide by 0.167 mm (one third of the window width) and analyze a window from 13.167-13.67 mm and see how many flame images fell within that range of heights. This process repeated until all images were classified by what bin window they fell under. The most populated "bin" of flame heights was characteristic of the images that were considered in the next step of image analysis. It was noted that the flame images captured by the 650 nm camera appeared shorter

than their 900 nm counterparts even though both cameras were spatially calibrated as closely as possible. This occurred because at higher temperatures such as those of a flame, a greater amount of light energy is emitted at higher wavelengths; therefore, images captured by the 900 nm camera appeared taller. Since the 650 nm flame images appeared shorter, only images captured by the 650 nm camera were used for consideration in the sliding bin analysis. All of the propane runs performed in a single day of testing were considered when selecting the images from each test set to be used for temperature profile extraction (i.e. photos from all propane runs performed in a single day of testing were processed when determining which flame images were best to be used to get temperature profiles).

An additional MATLAB code was utilized to determine each flame image's profile widths at set heights. The code analyzed each image's intensities at the heights of interest which were 54% and 70% of the total flame height, determined the location where the maximum intensity occurred and finally, determined the flame width based on the locations on each edge of the flame (in pixel space) where the intensities decreased to 2% of the maximum intensity as illustrated in Figure 13.

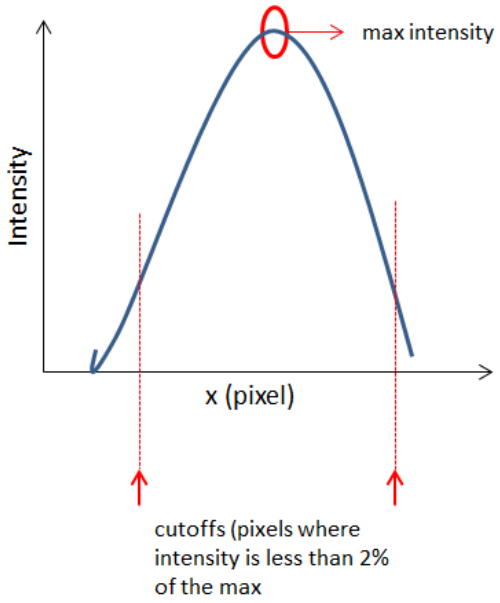

Figure 13-Illustration of how flame images profile widths were determined

The indicated profile width for each flame image was increased by 15 pixels when extracting intensity profiles to ensure that the flame profile width extended just slightly past the edges of the flame so that the most accurate Abel transform was obtained.

After the flame image profile widths at the heights of interest were determined, a scatterplot was generated for each group of images from one particular height. This allowed for a visual representation of the profile widths of each flame image's corresponding 650 nm image and 900 nm image (each data point represents one pair of images). An example is shown in Figure 14, the dark circles represent the image pairs that were used for temperature profile analysis.

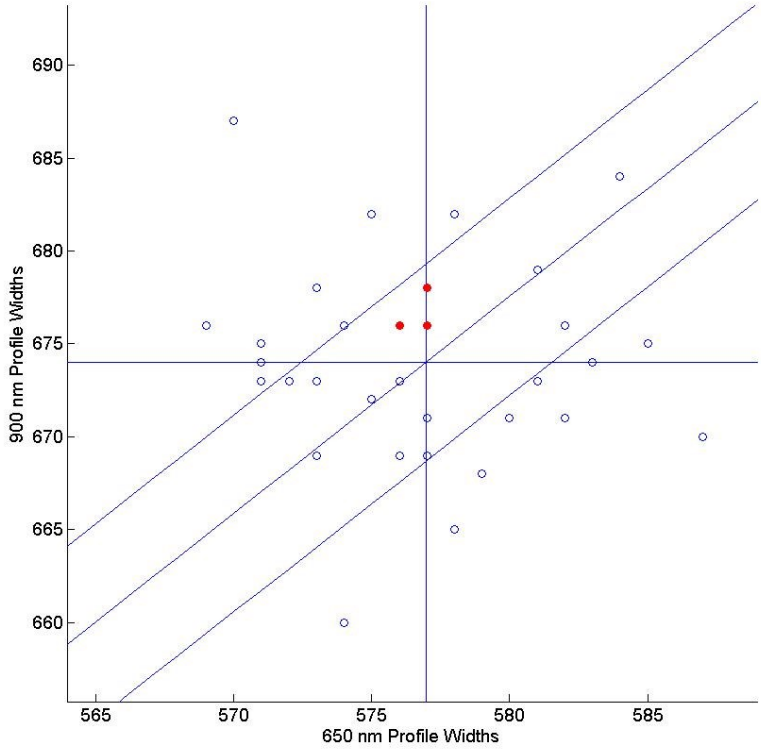

Figure 14-Scatterplot of propane flame image profile widths at 54% of the flame height

The x-axis represents the profile widths for the 650 nm images, while the y-axis represents the profile widths of the corresponding 900 nm images. The lines perpendicular to the x and y axes represent the mean profile widths for each wavelength's images. The scatterplot served as a visual indication of fluctuations in flame dimensions, and it was evident that points close to the mean profile widths were indicative of non-distorted images. Based on the observation that the mean 650 nm profile widths were consistently smaller than their 900 nm counterparts, it was evident that a symmetric image pair with a longer 650 nm profile width also had a longer 900 nm profile width partner and vice versa. This finding suggested that points that fell outside of a certain region associated with this trend represented flames that were not truly axisymmetric, and rather were ovular in shape at certain

points in time which can occur from pulsations in the flame even if the flame is laminar (Shaddix C. R., 2005). To determine the boundaries for acceptable flame images, a line of symmetry which passed through the intersection of the mean profile width lines was plotted on the scatterplot, and image pairs with profile widths that fell within +/- 7 pixels of the symmetry line were chosen for temperature profile analysis. The line passing through the intersection of the mean profile widths served as an indication of which image pairs had a linear proportionality of profile widths which was indicative of an axisymmetric flame. This method of image pair selection ensured that image pairs followed the expected trend in profile width for an axisymmetric flame in that an increase (or decrease) in profile width of the 650 nm image should also correspond to the same trend with the 900 nm image match. Flame image pairs that were closest to each other and closest to the mean profile widths of each wavelength were selected for the final data analysis.

Each selected pair of images was used to generate a temperature profile at the same height of interest used when analyzing profile widths. Since individual flame image intensity profiles varied in width, the MATLAB code which generated the plots of individual temperature profiles shown together was written so that the profiles were truncated to a common width for each pair. The process of determining flame image profile widths for the selection of images used in the final temperature profile analysis was repeated for each additional height of interest.

3.2 Propane Results

Propane tests were conducted in the MFC with five different sets of images captured per test, and flame image data was analyzed for all five sets of images to

determine temperature profiles from the best sets of images. Only image pairs that were symmetric with respect to the MFC burner, of similar height, and close to each other and close to the mean profile widths were considered for temperature profile analysis. The Abel transform tool in Spotlight was used to extract radially distributed intensities of each flame image at each of the two heights of interest. A smoothing factor of 10 which decreased the amount of noise (Klimek & Wright, 2004) and a line thickness of 2 were used to obtain more of a smoothed out profile without compromising the original shape of the transform. At first, the "calculate each side separately" option was used when obtaining the Abel transform intensities for an image, and the x pixel associated with the centerline of the image was approximated by eye as best as possible. The two maximum intensities were determined upon extraction of the deconvoluted intensities, and the average of the x pixel locations of these two max intensities was deemed the true centerline of the flame image as illustrated in Figure 15.

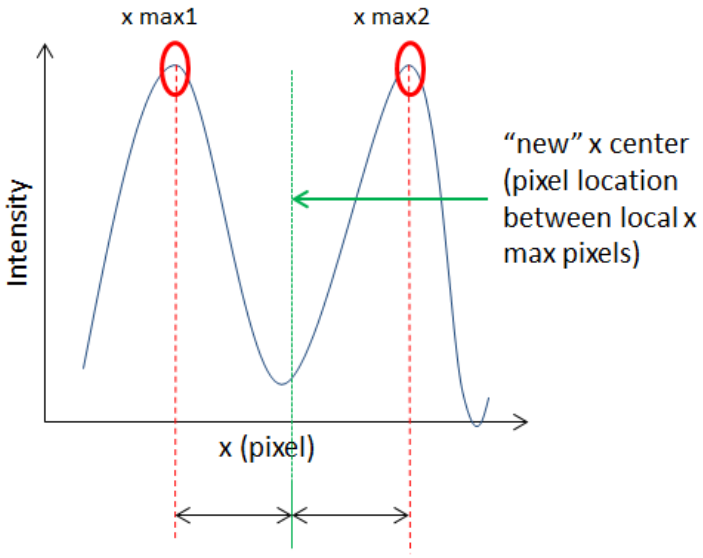

Figure 15-Illustration of how the true x center pixel value was determined based on Abel transform results with right and left sides calculated independently

The Abel transform tool was then re-centered in Spotlight at the determined x pixel centerline location, and the "average both sides" option was selected to obtain the radially distributed flame image intensities used in the temperature profile calculations. This process was repeated for each image. Figure 16 shows an example of the radially distributed intensities of two propane flame images obtained in Spotlight at 70% of the flame height.

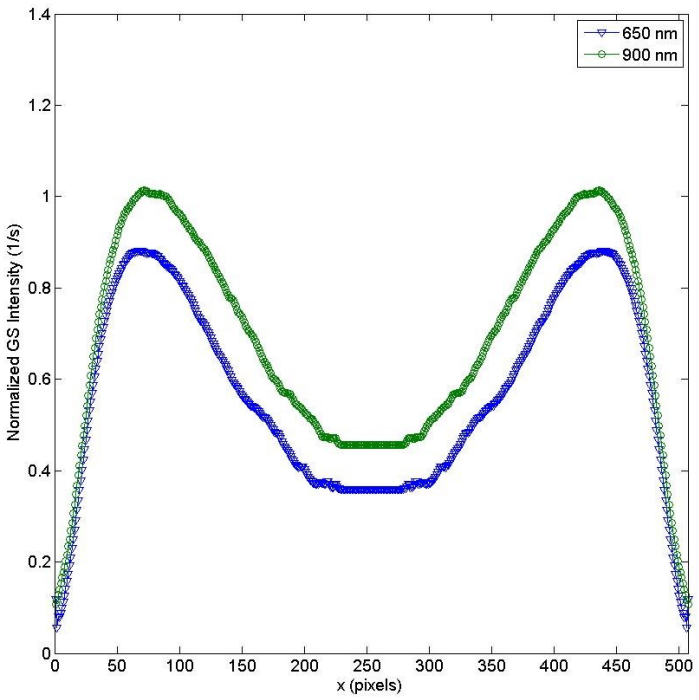

Figure 16-Example of Propane flame radially distributed intensities at 54% of total flame height

Originally, temperature profiles were plotted as an average of individual temperature profiles with error of the mean shown, but flame width varied a bit between different images pairs, so temperature profiles are shown as individual temperature profiles from individual sets of image pairs. In this fashion, averaging out maximum temperatures was avoided since peak temperature values of certain

profiles were “lost” when they resulted from a flame that had a more narrow profile width as compared to a wider profile. Shown in Figures 18 and 19 are the two temperature profiles obtained for propane at 54% and 70% of the image flame heights. Note that the temperature profiles have been truncated and cutoff values for edges of the temperature profiles were at the intensities values that were less than 10% of the value of the difference between the maximum and minimum intensity values. Truncating the temperatures profiles in such a manner was performed because regions near the center and edges of the flames had low soot concentrations, therefore, the ratio pyrometry method (which relies on ample soot presence) was not reliable in those regions. Figure 17 shows an example of a propane flame image pair that satisfied all aforementioned criteria and was used for temperature profile analysis.

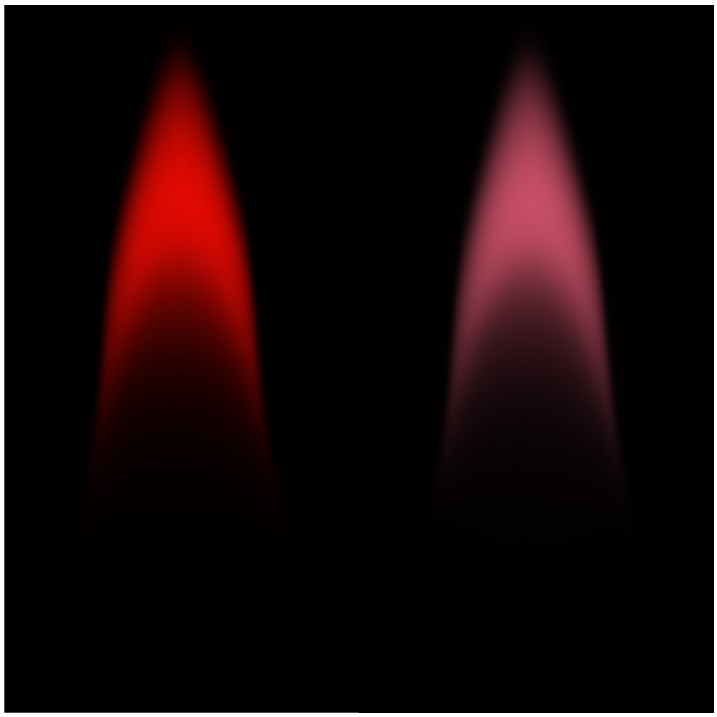

Figure 17-Example propane flame image pair

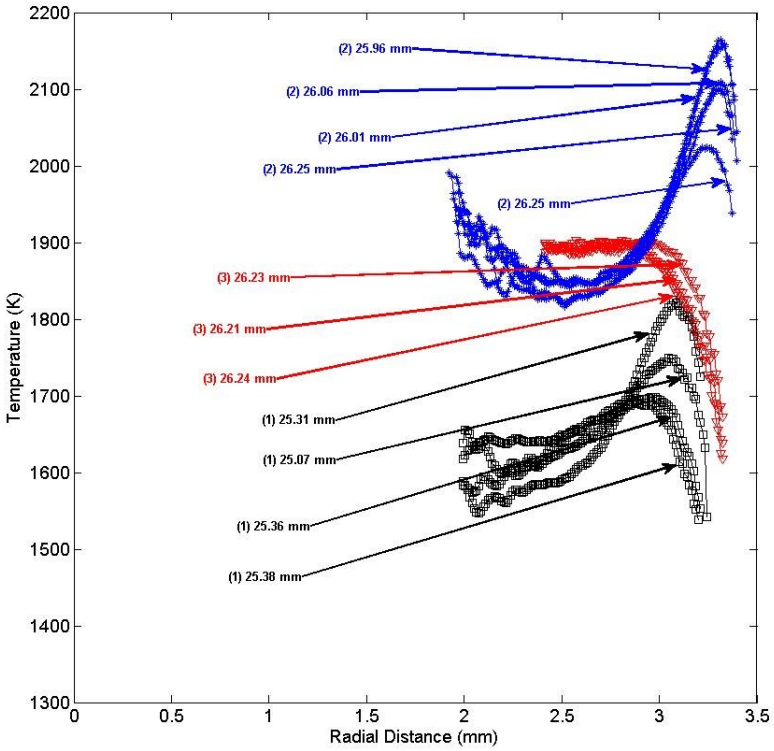

Figure 18-Temperature profiles of propane at 54% of total flame height for test days (1), (2) and (3) with total flame height indicated

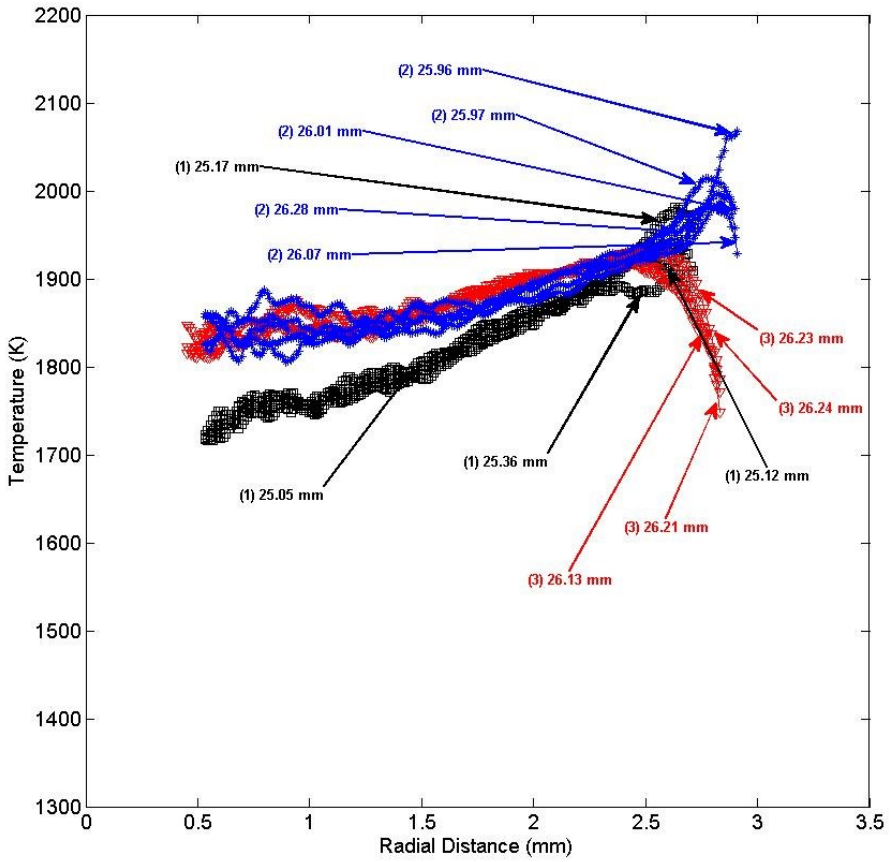

Figure 19-Temperature profiles of propane at 70% of total flame height for test days (1), (2) and (3) with total flame height indicated

In the temperature profile analysis of the solid fuels, 54% and 70% of the total flame heights were used as the heights of interests since these locations had high enough of a soot concentration to obtain data, yet were sufficiently far apart to obtain data for comparison at different heights in a single flame. For consistency, propane temperature profiles were also obtained at both 54% and 70% of the flame height; however, at the higher flame height, there was a greater concentration of soot. As mentioned previously, since the non-intrusive temperature measurement method used in this work is dependent on the presence and analysis of soot in flames, the

temperatures obtained at 70% of the propane flame heights are a better source of comparison to temperature values obtained from thermocouple measurements, which are described in the subsequent section.

Results from the propane tests were consistent with each other and had minimal differences in peak temperature values. The peak propane flame temperature at 54% of the flame height was about 1920 K, and peak flame temperature at 70% of the total flame height was about 1940-1950 K. Propane flame temperature measurements were then determined with a thermocouple as a final step of validation of the non-intrusive technique for flame temperature measurements in the MFC

3.3 Thermocouple Measurements

3.3.1 Materials and Methods

Thermocouple measurements of the propane flames were executed in order to compare experimental temperature profile results from the Nikon cameras to those obtained from a commonly utilized method of temperature data extraction. Thermocouples are widely used in the combustion and related communities for temperature measurements due to their accuracy and relative ease of use. Thermocouples are composed of wires with a welded junction which translates a voltage output to a temperature value through signals which are sent to the data acquisition system associated with the thermocouple (Ma & Long, 2012). Originally an S-type platinum-rhodium thermocouple (Omega Engineering part P10R-010-BW) with a wire diameter of 0.01" (254 μm) was selected for temperature measurement extraction; however, it was difficult to determine the actual temperature

of the flame based on unknown properties that were necessary to account for heat transfer corrections on the thermocouple. Although it also had a fairly small wire diameter, the S-type thermocouple also disrupted the structure of the flame as shown in Figure 20 in the example image captured by the SLR camera that captured images at 900 nm

Figure 20-Distruption of propane flame during thermocouple test

Thermocouple temperature measurements were attempted near the region between the middle and edge of the flame where it was hypothesized that high soot concentrations would occur yielding higher temperature results; however, when measurements were attempted in this region, it was difficult to position the thermocouple inside the flame due to the flame's tendency to "dimple" around the thermocouple wire junction. Although the thermocouple wire was fairly thin, the thermocouple's tendency to disrupt the propane flame structure combined with

difficulty in determining accurate heat transfer corrections served as reasons to re-try thermocouple measurements with a device that had a thinner wire diameter.

Attempts at improved propane thermocouple measurements were conducted using an unsheathed R-type platinum-rhodium thermocouple with wire diameter of 0.001” (25.4 μm) (Omega Engineering part P13R-001, shown in Figure 21 assembled with male connector and ceramic tubing).

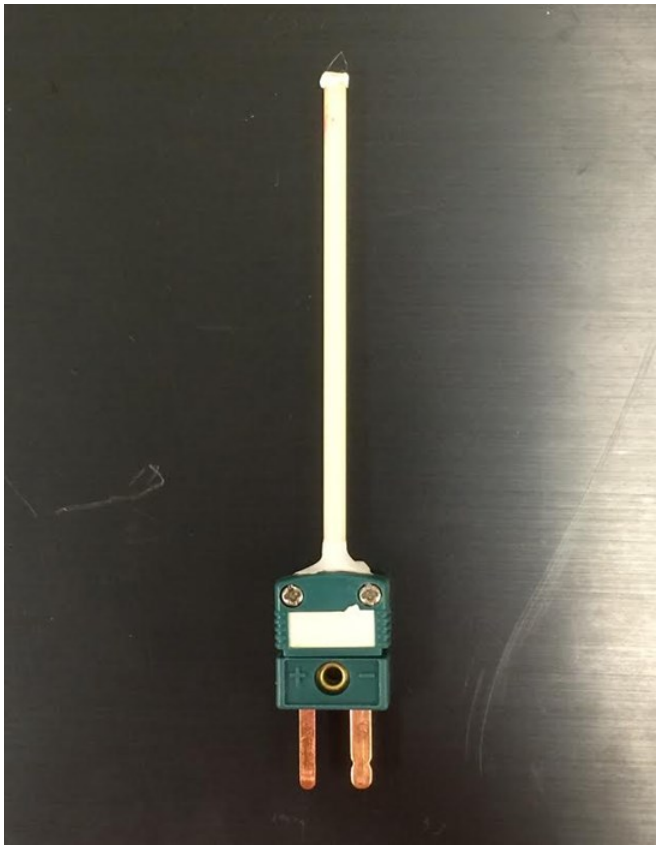

Figure 21-R-type thermocouple assembly

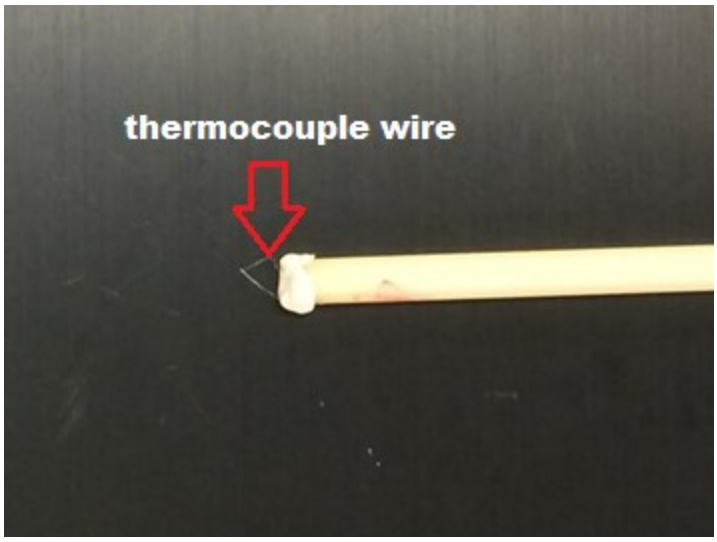

Figure 22-Close-up of R-type thermocouple wire and junction

The R-type thermocouple was advantageous due to its small wire diameter that was 1/10 of the original S-type thermocouple and the fact that it did not significantly disrupt the propane flame structure and was also able to withstand and record high temperature values of fuel flames. The photo in Figure 23 shows the R-type thermocouple penetrating the edge of a propane flame without causing significant "dimpling" of the flame edge or disruption of the flame's physical structure as was evident in previous experiments. Note that the image was captured with a non-modified digital camera for visualization purposes only and was not used at any point in time for data extraction.

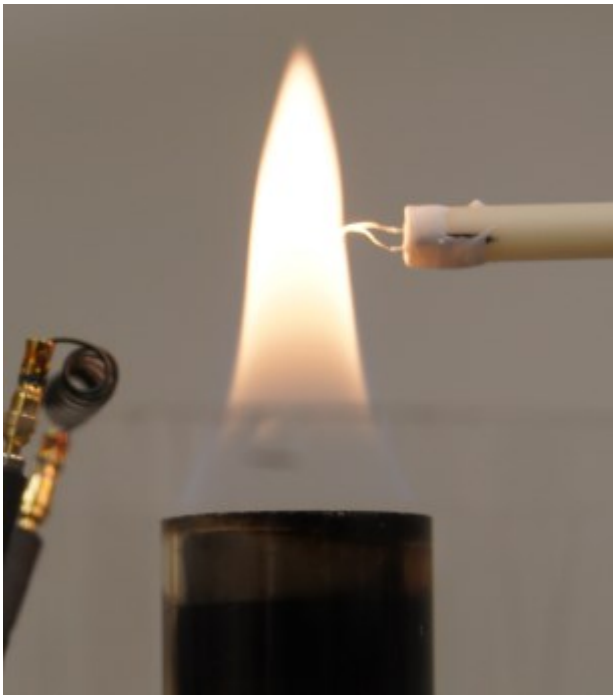

Figure 23-R-type thermocouple interaction with propane flame

Given its ability to withstand the propane and other flame temperatures up to about 2000 K without failing (Shaddix C. R., 1999), the R-type thermocouple was deemed an appropriate tool for extracting temperature measurements in this project.

3.3.2 Heat Transfer Corrections

As with any thermocouple measurement, determining the appropriate temperature correction based on heat transfer correlations was essential. In the context of combustion, heat transfer interactions in and around thermocouples include catalytic reactions at the thermocouple surface, conduction in thermocouple wires, and convective heating or cooling through transient heat transfer as illustrated by the schematic below (Shaddix C. R., 1999)

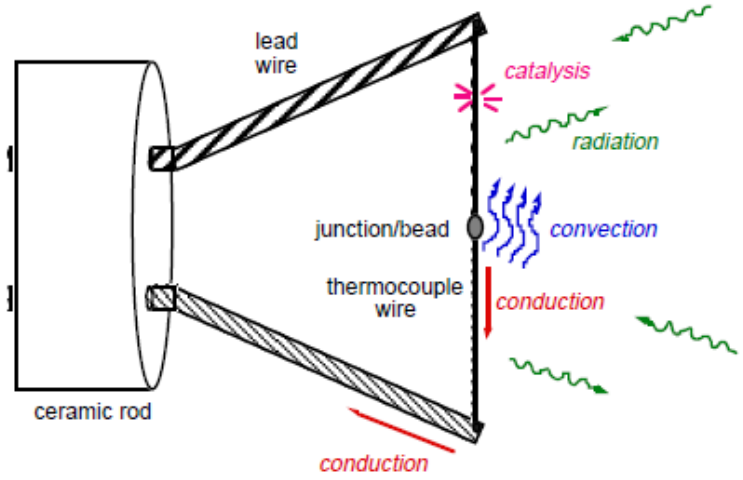

Figure 24-Illustration of heat transfer in a thermocouple in the context of combustion

A generalized energy balance on this system yields

$$\dot{Q}_{cat} + \dot{Q}_{conv} + \dot{Q}_{rad} + \dot{Q}_{cond} = \rho c_p V \frac{dT_{TC}}{dt} \tag{6}$$

In the application of the R-type thermocouple used in this project, as in similar applications, the convective term is the dominant mode of heat transfer, so effects of catalytic and conduction losses may be neglected, which is advantageous due to the difficulty of obtaining these values. Radiation effects; however, are considered due to their dependence on temperature to the fourth power. The overall energy balance necessary to determine experimental flame temperature simply reduces to a balance of convective and radiative heat transfer given by

$$h\left(T_g - T_{TC}\right) = \varepsilon_{TC}\sigma(T_{TC}^4 - T_w^4) \tag{7}$$

Given that the Nusselt number is defined as $Nu \equiv hd/k$, h may be expressed as $h = Nu * k/d$, and the expression for the flame temperature based on the thermocouple reading becomes

$$T_g = T_{TC} + \varepsilon_{TC}\sigma(T_{TC}^4 - T_w^4)d/kNu \tag{8}$$

Where

T_g is the gas, or flame temperature, in Kelvin

T_{TC} is the temperature reported by the thermocouple, in Kelvin

ε_{TC} is the emissivity of the thermocouple, unitless

σ is the Stefan-Boltzmann constant, 5.670e-8 W/m^2K^4

T_w is the wall, or ambient temperature, 298 K

d is the thermocouple wire diameter, 25.4 μm

k is the heat transfer coefficient, estimated as that of air at T_{TC}, in W/mK

Nu is the Nusselt number, unitless

A commonly used Nusselt number correlation for a cylinder (Shaddix C. R., 1999) was used since the application involved a low Reynolds number and a fine wire thermocouple. The cylinder Nusselt number correlation is used over a spherical correlation in the context of combustion since the Nusselt number correlation for a sphere does not generate reliable data based on previous experiments (Shaddix C. R., 1999). The correlation for a cylinder is given in Equation (9) (Collins, 1959)

$$Nu_{d,cyl} = \left(0.24 + 0.56Re_d^{0.45}\right)\left(\frac{T_m}{T_\infty}\right)^{0.17} \tag{9}$$

T_m, the film temperature was assumed to be the same as the ambient temperature, so the T_m/T_∞ term reduced to 1, making the Nusselt number solely dependent on the Reynold's number given by

$$Re_d = \frac{\rho u d}{\mu_{gas}} \tag{10}$$

Where

ρ is density, estimated as density of air at T_{TC}

u is velocity of the fuel flow, in m/s

d is the wire diameter, 25.4 μm

μ is dynamic viscosity, estimated as viscosity of air at T_{TC}, in N-s/m^2

The flow velocity of the fuel was estimated under the assumption that the flame was buoyancy-driven. Through simple kinematics, velocity may be expressed as

$$u = \sqrt{2 * a * x} \tag{11}$$

Where x in this case was the height of interest of the flame, which was usually between 15 and 20 mm. In the case of buoyancy-drive flow, acceleration, a is given by (Turns, 2012)

$$a = 0.6g(\frac{\Delta\rho}{\rho}) \tag{12}$$

Where $\frac{\Delta\rho}{\rho} = \frac{\rho_\infty - \rho_F}{\rho_F} = \frac{T_F - T_\infty}{T_\infty} = \frac{T_F}{T_\infty} - 1$, making acceleration of the flame result to

$$a = 0.6g(\frac{T_F}{T_\infty} - 1) \tag{13}$$

Where

T_F is the flame temperature, estimated as the reported thermocouple temperature

T_∞ is the temperature of ambient air, 298 K

g is acceleration due to gravity, 9.81 m/s^2

Based on this expression for acceleration, flow velocity was determined in multiple cases to be about 1 m/s based on varying thermocouple reported measurements on the order of about 1800 K and flame heights of about 15-20 mm. A velocity value of 1 m/s was then used in subsequent cases when calculating thermocouple heat transfer temperature corrections.

For an R-type platinum-rhodium thermocouple, ε_{TC}, thermocouple emissivity is approximated based on thermocouple temperature as shown in Equation (14)

$$\varepsilon_{TC} = 1.507e-4 * T_{TC} - 1.596e-8 * T_{TC}^2 \quad (14)$$

Laboratory tests conducted by Honeywell Research Center showed that this relationship is in good agreement with experimental results (Ang, Pagni, Mataga, Margle, & Lyons, 1988). Given this relationship, it was possible to obtain all parameters necessary to solve for the thermocouple correction temperatures.

3.3.3 Results

Propane flame temperatures were measured with the R-type thermocouple, and the actual flame temperatures were determined based on heat transfer corrections. Measurements were taken near the edge of the propane flame at about 70% of the total flame height. Several individual temperatures were obtained at various points in time and then averaged to get a reported temperature of the propane flame at that location. The results of these tests are shown in Table 2

Table 2-Propane flame temperature values obtained from thermocouple

Location	Reported Temperature (K)	Radiation Corrected Temperature (K)
Flame Edge	1770	1900

The reported temperature values in the graphs were a representative average of multiple flame temperature measurements taken over a period of several minutes since the LabVIEW program used to collect thermocouple data had a 1 Hz sampling rate. With the given temperature corrections for the R-type platinum-rhodium thermocouple, the maximum average propane flame temperature was about 1900 K.

The maximum propane flame temperatures near the flame edge obtained from the temperature profiles using the non-intrusive method were on the order of about 1965 K at 70% of the total flame height based on the arithmetic mean of the peak temperature values. The differences in propane flame temperatures between the thermocouple reading of about 1900 K near the edge of the flame and the maximum temperatures from the non-intrusive method were about 65 K at 70% of the flame height. Note that the thermocouple value of 1900 K was obtained at one particular flame height of about 19 mm on the flame which was closer to the location at 70% of the flame height analyzed with the non-intrusive method. At this location, the difference between the maximum flame temperature obtained using the ratio pyrometry method and the average thermocouple temperature was about 65 K which was low enough of an error to serve as acceptable criteria for validation of the non-intrusive flame temperature measurement technique, given that the error for thermocouple measurements alone is about 50-100 K (Shaddix C. R., 1999). Since propane flame temperature results were consistent and repeatable between two methods of measurement, focus was then directed to obtaining flame temperatures of polymer fuels using the non-intrusive method with D-SLR cameras.

4. Polymer Tests

4.1 Experimental Design

4.1.1 Revisions to Technique

The general arrangement of the MFC was the same in polymer tests as in the propane tests except for a few minor differences. Since solid fuels were pyrolyzed and prompted to combustion, propane gas was no longer connected to the MFC and instead was replaced with Nitrogen gas. The coil of the igniter was also removed from the set-up as to avoid disruption of the flame as was observed in tests during MFC development and experiments (Ding, 2013). To prompt ignition, a hand-held blowtorch was used as a piloted ignition source and removed at the earliest detection of a polymer flame. A schematic diagram of the MFC as used in polymer tests is shown in Figure 25

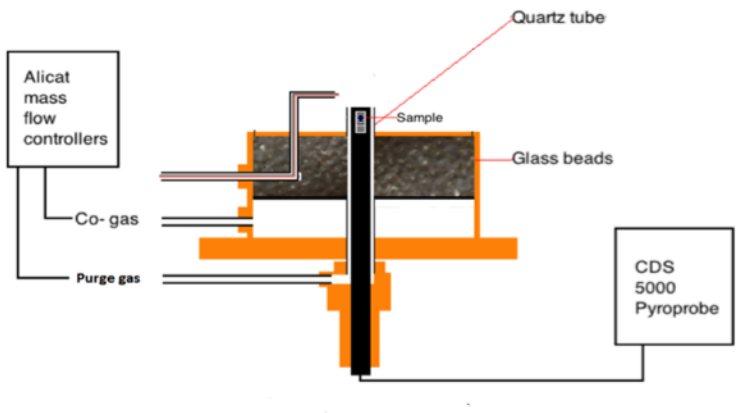

Figure 25-Schematic of MFC as used in polymer tests

Samples used in polymer runs were consistently massed to 30 mg +/- 1 mg in a glass sample tube to assure that experiments were as repeatable as possible and not skewed by differences in mass between sample tests. All polymer samples were also conditioned in a desiccator box for at least 48 hours prior to experiments to allow for optimal moisture removal.

Similar to propane flame tests, during polymer runs, a lid made of flame resistant PVC material was placed on top of the MFC "cage" to create the best seal possible around the flame to prevent flickering and prompt flame stability. Especially during brominated flame tests, a fair amount of soot was produced during pyrolysis, so immediately after flame images were captured, the PVC lid was removed. This allowed for ventilation of soot and gases produced from polymer flames since the

stability of the flame was no longer a concern after the D-SLR cameras had acquired flame images.

Polymer samples were pyrolyzed using a CDS 5000 Pyroprobe with a prescribed heating rate of 10°C/s and a maximum temperature of 1200°C. The aforementioned hand-held blowtorch was used as a piloted ignition source and removed immediately after a flame was detected. Nitrogen gas at a flow rate of 100 SCCM was supplied to the quartz tube which enclosed the pyroprobe and polymer sample in the sample tube to encourage combustion, and air supplied at a flow rate of 4 SLPM was used as the co-flow gas in each experiment to help stabilize the flames. Prior to each set of experiments, the system was pre-heated by flowing the Nitrogen and air gases while the pyroprobe ran and reached its maximum temperature without a contained sample.

4.2 Image Acquisition

Unlike in the propane experiments, the polymer samples had mass loss rates associated with them which meant that the flame was not virtually identical at various points in time, and mass flux was not constant. This presented a challenge since there was a limited amount of time available to capture adequate polymer flame images for analysis since these flames had a time dependence associated with them. In the propane experiments, pictures could be taken at any point in time, but in the polymer experiments, images had to be taken at an optimal point in time since the flames' heights varied with time, growing initially and then slowly shrinking as sample mass was depleted. Based on videos of pure and brominated polystyrene, optimal times for capturing flame images for each polymer post-ignition was determined based on the

regions where the flames were fairly steady, as will be discussed in further detail in subsequent sections. Figures 26 and 27 show the progressions of polymer flame heights with respect to time for three separate tests as recorded by an unfiltered Sony camera.

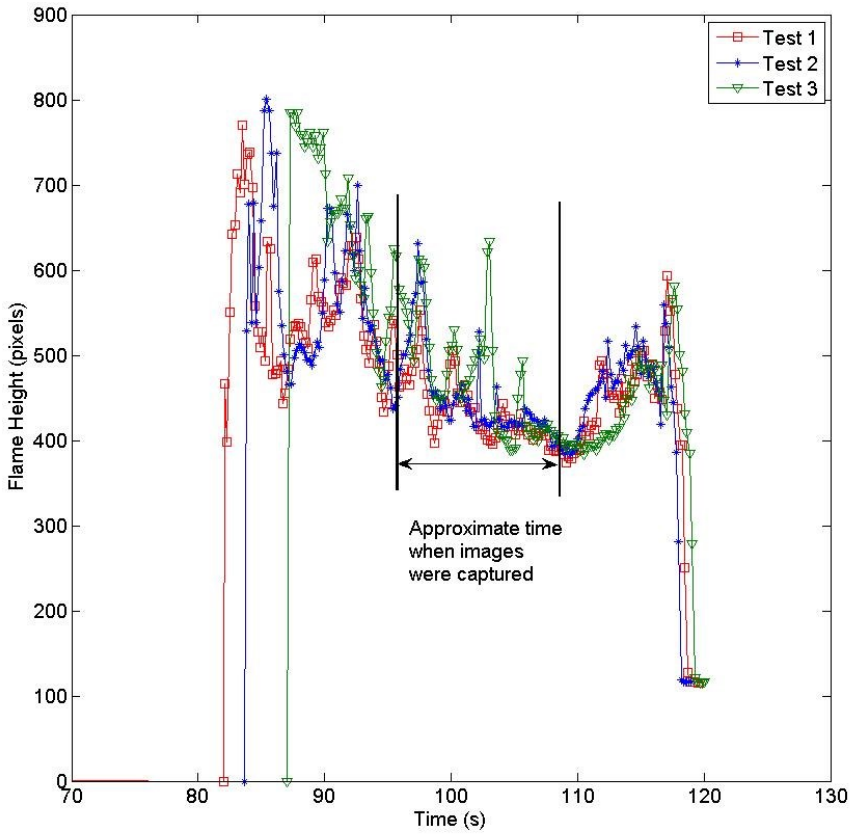

Figure 26-Flame height progression with time for three PS flames based on analysis of unfiltered videos

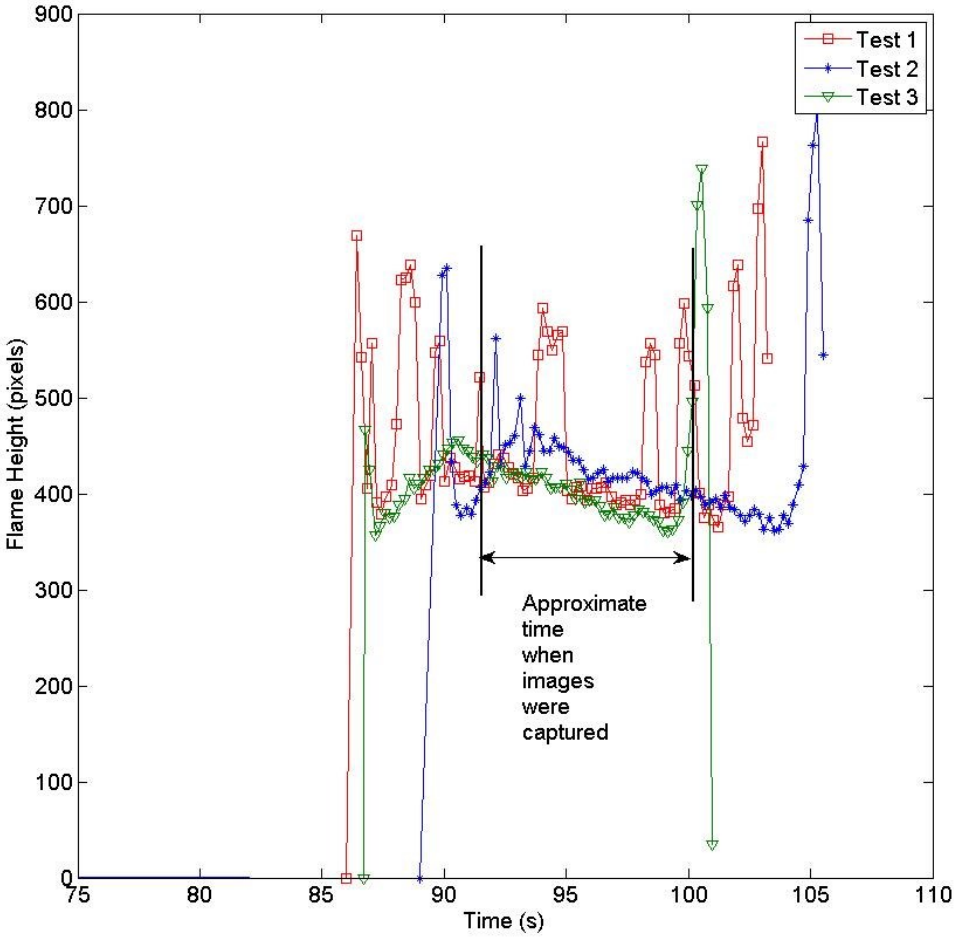

Figure 27- Flame height progression with time for three PSBr flames based on analysis of unfiltered videos

After the designated post-ignition delay, 10-15 images were captured by the two Nikon cameras in single frame shooting mode set to a rate of 1 picture per second in the Triggertrap "Timelapse" mode. Single frame shooting mode was used in all tests since flame images were captured at identical points in time in "slow" mode. A limitation of this shooting mode was that bursts of images could not be captured, and it took longer to acquire polymer flame images when time was a more sensitive parameter in experiments.

4.3 Image Analysis

As mentioned previously, the optimal time delay for acquiring flame images after ignition was determined using a MATLAB code which analyzed videos of both pure PS and PSBr from before ignition until burnout. The code analyzed the intensities of the flame in each video along the approximated centerline of the burner. The cutoff for the tip of the flame was the location where the intensity along the centerline of the flame decreased to 30% of the maximum intensity since a different visual camera was used to collect flame videos, and intensities from the camera were different due to different camera setting. A graphical representation of the flame height progression with respect to time was then obtained to allow for determination of the region in time where the flame height was roughly constant, as shown previously in Figures 26 and 27.

For the PS samples, ignition was detected at roughly 84 seconds, and the flame stabilized reaching a roughly constant height at about 96 seconds which was about 12 seconds after ignition. Roughly constant flame height still held about 10 seconds later, so 12 seconds after visually detected ignition was used as the delay before capturing images of PS flames.

The PSBr flames appeared to be artificially tall at the end of pyrolysis because the flames exhibited a "liftoff" behavior at the point of extinction. As the PSBr flames extinguished, instead of steadily shrinking, the edges of the flame curled upwards in a manner that appeared to lift the flame until it spontaneously extinguished. PSBr samples ignited approximately 87 seconds after the start of pyrolysis, and at about 91 seconds post-pyrolysis, the flames reached a relatively

consistent height, so the same delay of 4 seconds was implemented during experiments before the Triggertrap device was activated to capture flame images. Capturing images of PSBr shortly after detected ignition was advantageous due to the fact that the bromine presence in the flames may not have been as prominent later in combustion as the flames drew closer to extinction.

Three different days of polymer tests were done with cameras re-calibrated between tests, and each test was composed of three individual PS runs (nine PS samples total were tested). The best pairs of 650 and 900 nm flame images used for temperature profile analysis were determined based on the same image analysis criteria as in the case of the propane flames as illustrated in Figure 11 and described in section 3.1. The first filter was flame angle. The angle of each flame image was identified using a MATLAB code similar to that used in the propane image analysis. The code extracted a line profile of intensities across the flame images at 70% of the total flame height on both the left and right sides of the centerline of the flames, assumed to be the x pixel location of the burner. The two locations where the maximum intensities occurred on the flame (one on the left side, one on the right) were averaged to identify the true x pixel location of the center of the flame. The distance between the true flame centerline and the center of the burner was compared to the angle formed with the plane of the base of the burner, so the closer the angle was to 90° the more symmetric the flame image was. Corresponding flame image pairs each with a flame angle of about 85° or better were considered symmetric.

Similar to the propane tests, polymer flame heights were determined by using a MATLAB code which analyzed the intensity of each flame image along the

centerline of the flame, assumed to be the x pixel location of the burner centerline determined from alignment calibration. The polymer flame images were brighter along the edges of the flames, most likely due to increased soot concentration, so the intensities along the polymer flame centers were not as high as in the propane tests. The cut off for polymer flame height was determined to be the pixel location along the centerline of the flame where the intensity decreased to 20% of the maximum intensity along the flame centerline since polymer flames were not as bright in the center of the flames as compared to propane flames. When a line profile of flame image intensities was drawn along the flame centerline, the intensity of the flame image at the pixel located very close to the top of the flame was about 20% of the maximum intensity detected along the centerline of the flame, so 20% of the max was used as the criterion for determining the polymer flame height.

Polymer flame images of similar heights were determined using the same "sliding bin" MATLAB code analysis as with the propane flames. The only difference was that the bin window width was increased to 1.5 mm since the polymer flames' heights varied more greatly than the propane flames.

The next filter used to determine the best flame image pairs for temperature profile extraction was flame width. The MATLAB code which was used to determine flame image widths at 54% and 70% of the total flame height was similar to that used in propane analysis, but examined a line profile of intensities across the heights of interested and used the "edge" function in MATLAB to identify the two locations on the flame edges where the maximum intensities occurred based on locations where image intensity gradients are the greatest (similar to before, one on

the left side of the flame, one on the right side). The distance between the two edges was the designated flame width, and an extra 15 pixels was added to the flame width at each height when data was extracted in Spotlight to ensure that the Abel transform tool captured the full width of the flame images, extending slightly past the edges. As in the case of the propane flames, a scatterplot of the widths of the 650 and 900 nm image pairs was generated, and image pairs that were closest to the mean profile widths and to each other were used to extract temperature profiles. Shown in Figure 28 is an example of a pair of PS images which satisfied all the criteria for optimal image analysis.

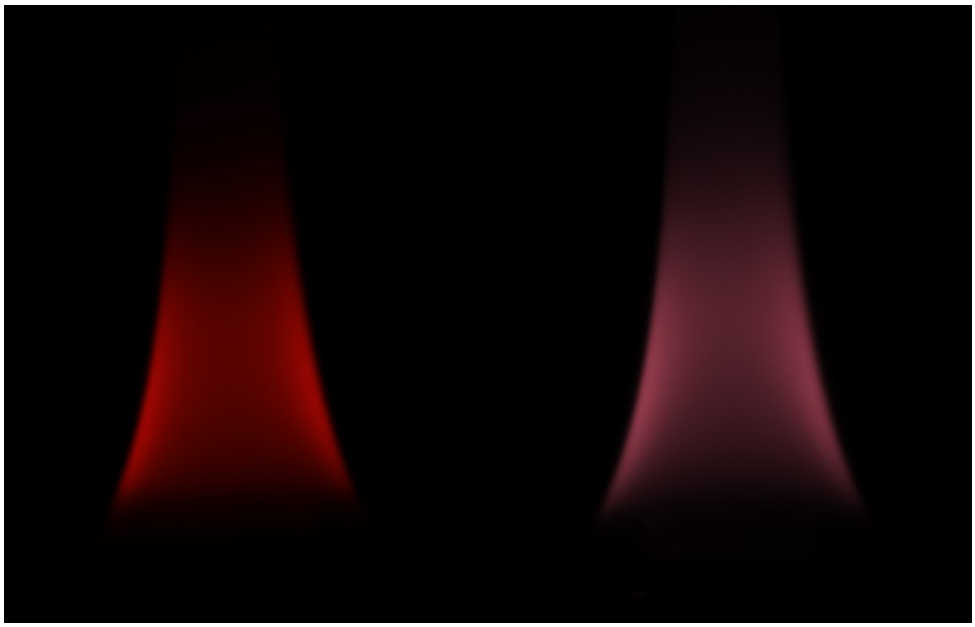

Figure 28-Example pair of PS flame images at 650 nm (L) and 900 nm (R)

4.3.1 PS Results

In the same fashion as with the propane data analysis, the Abel transform tool in Spotlight was used to extract intensities from each flame image that were necessary to determine flame temperature profiles. The Figure 29 is an example of the radial

distributions of the PS flames shown before at 54% of the total flame height. Due to the miniscule soot concentration and intensities at the center of the flames, the intensity values in this region were truncated to avoid values below zero.

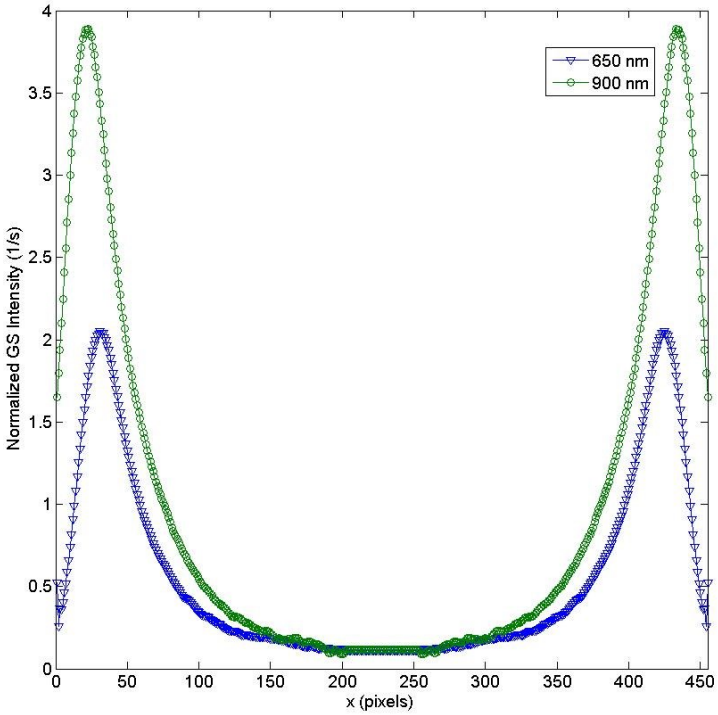

Figure 29-Example of PS flame radially distributed intensities at 54% of total flame height

The resultant temperature profiles for PS at 54% and 70% of the total flame heights are shown in Figures 30 and 31 for tests (1), (2) and (3). The time delay after the start of pyrolysis and total flame height (for the 650 nm image) are also indicated on each temperature profile.

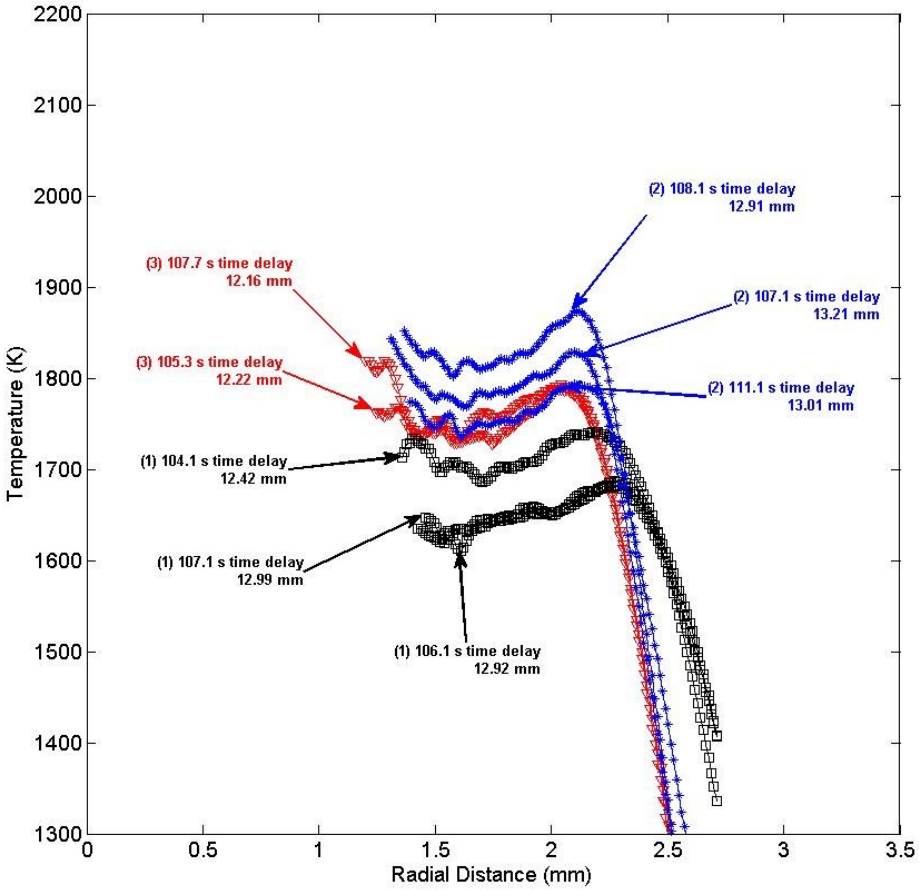

Figure 30-Temperature profiles of PS at 54% of flame height for test days (1), (2) and (3) with time delay from start of pyrolysis and total flame height indicated

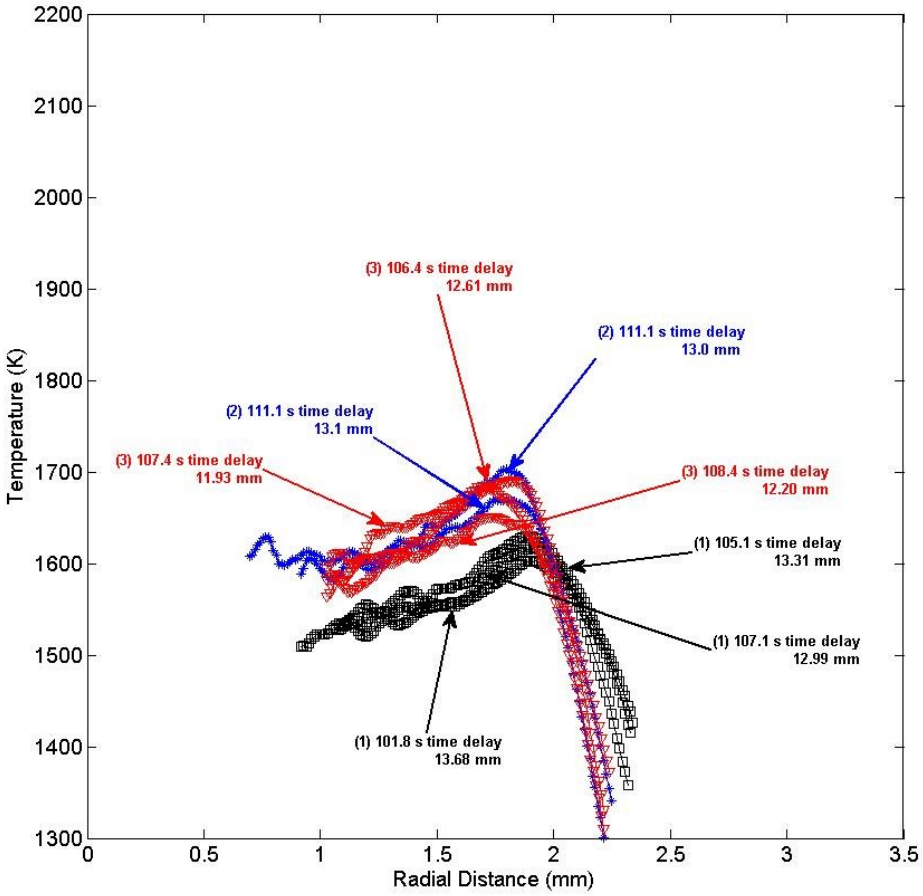

Figure 31-Temperature profiles of PS at 70% of total flame height for test days (1), (2) and (3) with time delay from start of pyrolysis and total flame height indicated

A bit of variation between some of the PS temperature profile widths was present, but peak temperature values occurred near the edges of the flames as expected since the greatest amount of soot was concentrated in that area. The general shapes of the PS temperature profiles were also the same despite a few differences in peak temperature values. Temperature profiles from the second (2) and third (3) tests agreed closely with each other with peak temperatures near the edges within about 50 K of each other. Differences in temperature profiles and peak temperature values may be attributed to differences in the point in time for which images were captured as well

variations in the total flame heights of images used to create each temperature profile. An analysis on effects of the constant of calibration was conducted for the PS temperature profiles at 70% of the total flame height to investigate whether or not the constant contributed to the differences in peak temperature values with results shown in Table 3. Note that two standard errors of the mean were used.

Table 3-Statistical analysis of effect of calibration constant on flame temperature profiles

Condition	Mean Max Temperature (K)	Error (K)
Individual calibration constants	1656	26
Single calibration constant for all profiles	1657	22

The mean peak temperatures were nearly identical and fell within each other's errors for the PS calibration constant analysis; therefore, the constant of calibration could not be contributed to the source of differences in temperature profiles.

4.3.2 PSBr Results

The brominated polymer sample analyzed in this work was composed of 60% BASF polystyrol 158K (pure PS) and 40% Saytex HP 3010 for a composition of 27.4% bromine by weight. For the PSBr samples, the same method for selecting the best pairs of flame images to be used for extracting temperature profiles was employed as in the case of the PS samples. The only difference was that the set size of the window used in the sliding bin analysis was 1 mm for some test days instead of

1.5 mm since the flame images of samples containing bromine tended to vary less in height. An example pair of PSBr flame images which satisfied all criteria is show in Figure 32

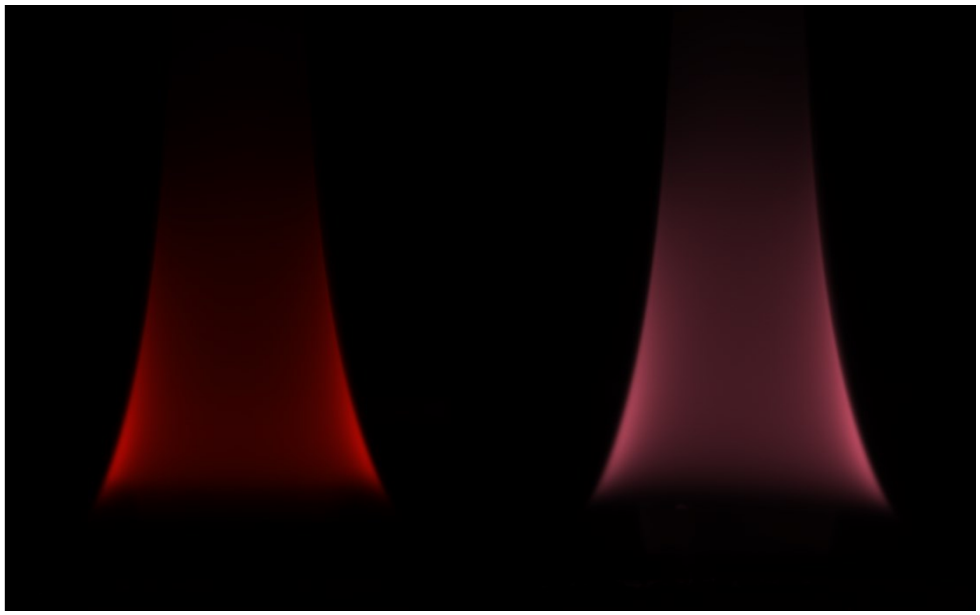

Figure 32-Example pair of PS-BR2 flame images at 650 nm (L) and 900 nm (R)

The PSBr temperature profiles obtained from three separate tests are shown in Figures 33 and 34.

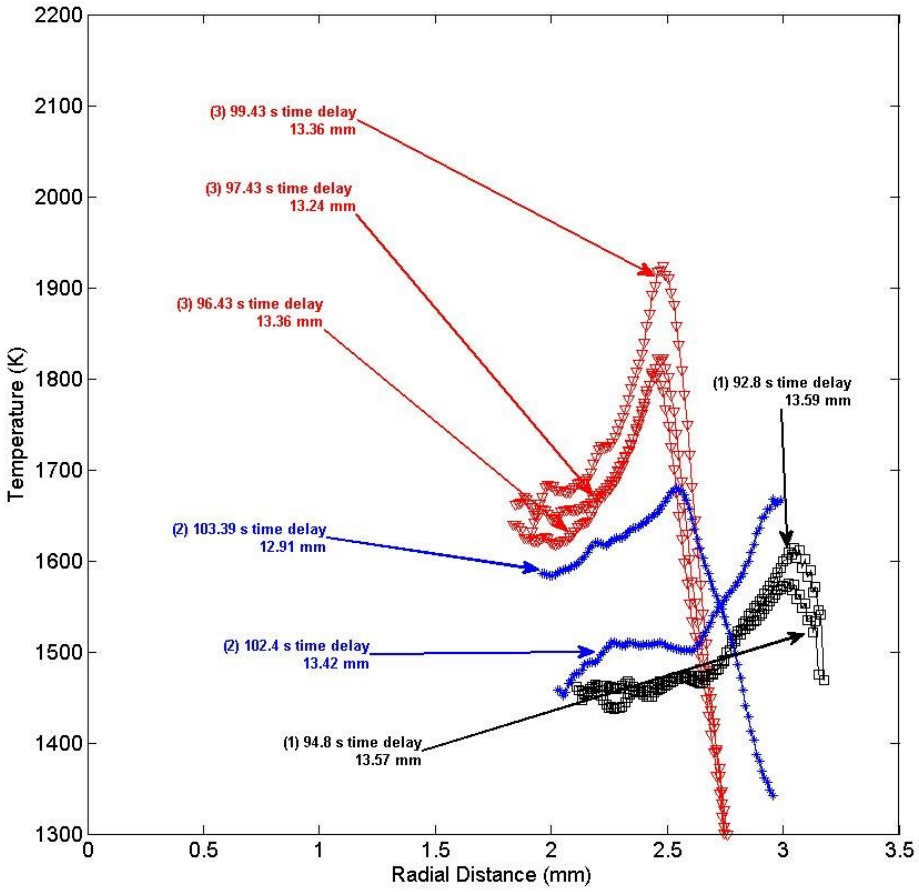

Figure 33-Temperature profiles of PSBr at 54% of flame height for test days (1), (2) and (3) with time delay from start of pyrolysis and total flame height indicated

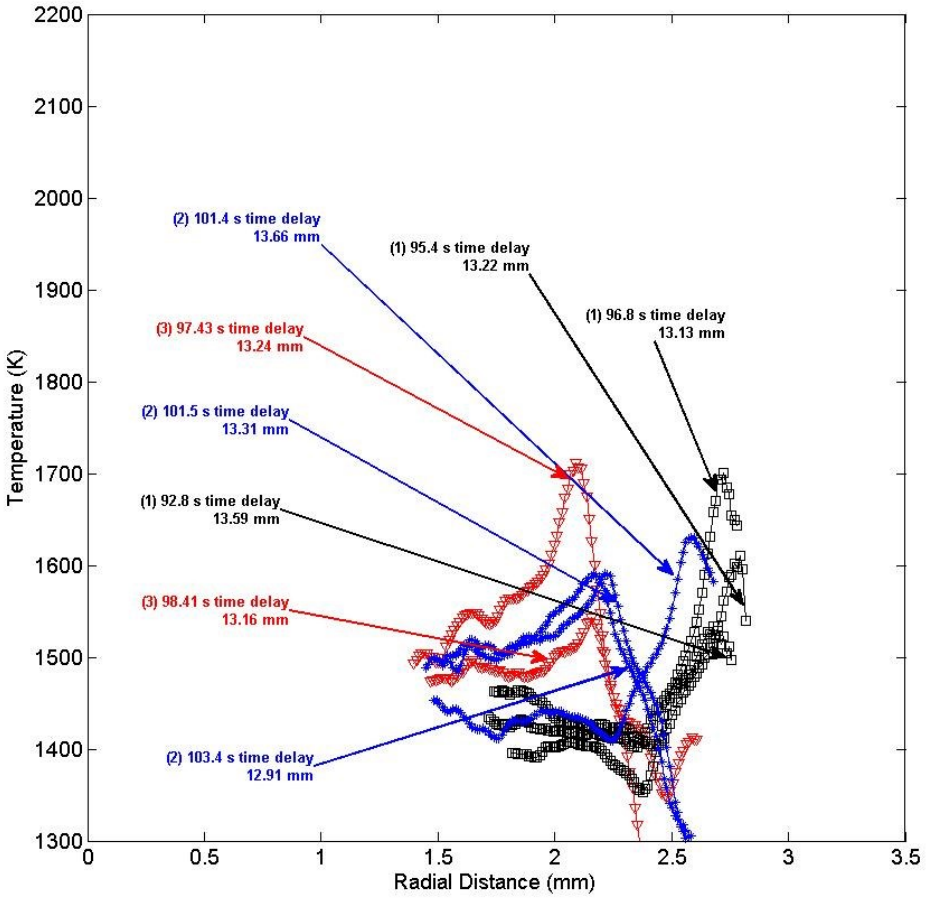

Figure 34-Temperature profiles of PSBr at 70% of flame height for test days (1), (2) and (3) with time delay from start of pyrolysis and total flame height indicated

Especially with the third (3) test data considered, the PSBr temperature profiles had greater variation between each other than in the case of the PS results. The PSBr temperature profiles obtained for the first (1) and second (2) tests at 54% of the total flame height were relatively consistent, and peak temperatures near the edges of the profiles were within about 75 K of each other, but the temperature profile results from the third (3) test were not as consistent with the previous test results. The PSBr temperature profile results obtained at 70% of the total flame height exhibited a variety of different overall shapes and widths, suggesting that the bromine-containing

polymer samples were more sensitive to what point in time flame images were captured; however, in the cases of the first two PSBr tests, the maximum temperatures were lower than those of the PS maximum temperatures at both heights, which is consistent with the hypothesized notion that the presence of a flame retardant would decrease the HRR and overall temperature of polymer flames.

Table 4 summarizes the critical statistics of the temperature profiles of the propane gas and polymer flames. The arithmetic mean and two standard errors of the mean were calculated for each of the flame temperature profiles based on the maximum temperature value of each individual profile.

Table 4-Statistical Analysis of Maximum Flame Temperatures

Material and Flame Height	Mean Max Flame Temperature (K)	Error (K)
Propane 0.54H	1935	+/- 100
Propane 0.7H	1966	+/- 26
PS 0.54H	1773	+/- 48
PS 0.7H	1656	+/- 26
PSBr 0.54H	1773	+/- 50
PSBr 0.7H	1614	+/- 46

The flame temperature measurements taken at 54% of the total flame height had the largest error, suggesting that measurements taken in this region are the least consistent; however, for the flame temperature profiles at 70% of the total flame height, the errors were much smaller despite the fact that the actual shapes and widths of the flame temperature profiles varied quite a bit.

5. Conclusions

5.1 Discussion of Results

5.1.1 Polymer Flame Temperatures

The PS flame temperature profiles displayed a bit of variation, but generally had the same overall shape with maximum temperatures near the edges of the flames where the greatest concentration of soot was present. Statistical analysis was conducted by analyzing the maximum flame temperature profile values and comparing their mean values as well as two standard errors of their means. These results are shown graphically in Figure 35. Since flame temperature profiles were not as consistent at 54% of the total flame height, especially for propane, only polymer flame temperature results at 70% of the total flame height were considered.

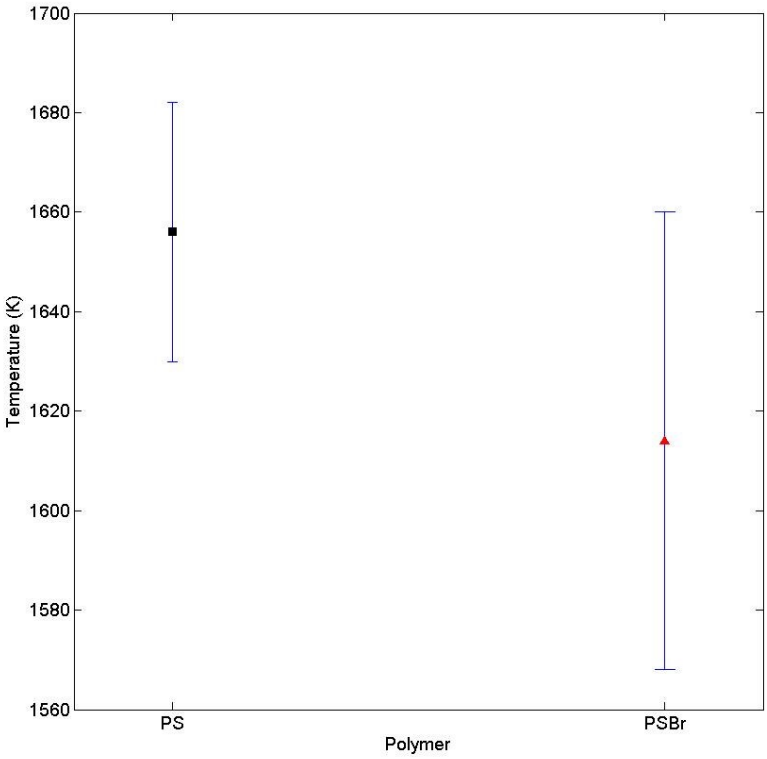

Figure 35-Mean maximum flame temperatures for PS and PSBr at 70% of total flame height

The average maximum flame temperature profile value for the PS flames was 1656 K while the maximum value for PSBr was 1614 K which suggests that brominated flame retardants may indeed decrease polymer flame temperatures as well as HRR; however, the errors of both flame temperatures fall within each other, so sufficient conclusions cannot be made solely based on the present data and further analysis is required.

In the cases of the PSBr temperature profiles, results were not as consistent as those obtained from the PS tests, therefore it is more difficult to begin to draw conclusions based on the observed variations in the data. The mechanism by which the bromine in PSBr is released during combustion may be the primary reason that such variations in temperature profiles are observed. The effects of the bromine

inhibiting flame propagation may be more pronounced at specific times during combustion so that resultant flame temperature profiles of PSBr flames exhibit a greater amount of variation since they appear to be more sensitive to the point in time when images are captured relative to the initiation of pyrolysis.

The linear heating rate of the pyroprobe may also have contributed to variations observed in the polymer flame temperature profiles. The pyroprobe heated the polymer samples at a constant heating rate, so it is possible that capturing images at slightly different points in time when the pyrobrobe was running resulted in variations in flame temperatures depending on the temperature of the nitrogen gas which was also heated by the pyroprobe. This also could have impacted the chemistry by which the polymer flames interacted with the surrounding environment and in particular, the timing and release of the halogen flame retardant material.

5.1.2 Practical Applications

Preliminary results of non-intrusive temperature measurements of propane flames were consistent and within reasonable agreement of thermocouple results, which suggested that the method could be utilized to extract polymer flame temperatures from samples pyrolyzed in the MFC. Although PSBr flame temperature results were not as consistent as pure PS results, the presented findings suggest that polymer flame temperatures may be measured non-invasively at the milligram scale, although further work is necessary to develop a stronger foundation of the method. The statistical analysis of PS and PSBr maximum flame temperature values at about 70% of the total flame heights also suggest that the use of bromine as a flame retardant in polymers decreases flame temperatures, and decreased flame

temperatures may also result in decreased HRR as it is related to temperature. Through further work, it may be possible to draw more concrete conclusions about effects of bromine on flame temperature since the errors from this work were too large to draw finite conclusions based on the statistics of PS and PSBr flame temperatures. Testing in the MFC was a practical way to obtain flame temperature profiles through ratio pyrometry since the required sample size for each individual run was only 30 mg, and is advantageous for future applications and testing.

5.1.3 Limitations

Previous work related to flame temperatures of polymers measured non-intrusively is not existent; therefore, one of the greatest limitations of the data is that it is has no predecessor for means of comparison. As mentioned previously, the gas-phase mechanisms of combustion related to interactions between the gas and solid phases are not well understood and little data exists to support a knowledge basis of such.

Polymer experiments themselves were limited in that only one picture per second could be captured, so only about ten flame images were captured for each individual run. After three runs per day of testing, once the appropriate methods of image pair selection were employed, only about 1-2 flame temperature profiles could be obtained for PS and PSBr after a full day of testing. The window of time available for capturing flame images was very limited which made it difficult to obtain a great deal of temperature profiles from a set of tests.

5.2 Future Work

5.2.1 Suggestions

The technique applied in this work is foremost, the first of its kind utilized in the context of polymer flame temperature measurements, and a greater amount of testing must be conducted to confirm the validity of the method and its results. Only pure and heavily brominated PS were considered in this analysis, so it would be interesting to see a greater variety of polymers tested in a similar fashion and compare the flame temperatures pure polymers with their flame retardant-containing counterparts.

An additional point of interest for future work would be to conduct tests in the MFC with the pyroprobe set to a constant heating rate. Samples usually ignited around 900°C, so exploring resultant polymer flame temperatures from experiments run with the pyroprobe at a constant heating rate once the approximate temperature of ignition was reached could eliminate the observed discrepancies that may have been attributed to the linear heating rate of the nitrogen gas.

A great deal of multitasking was necessary to effectively capture polymer flame images which were used in data analysis, and it was virtually impossible to conduct experiments in the MFC without the aid of an additional individual. It was challenging for a single user to record the time to ignition, apply a piloted ignition source and do so until ignition was detected, start a timer for the appropriate ignition delay before capturing images, signal the Triggertrap devices, and immediately remove the PVC lid over the MFC cage after image acquisition in a single polymer test. Employing a more sophisticated MFC that could run experiments in a more

automated fashion would allow polymer experiments to be conducted more easily by one user and eliminate some of the sources of error.

Conducting further experimental work with the MFC to measure polymer flame temperatures using ratio pyrometry would create a stronger foundation for a technique which can be more refined for use in further material testing and evaluation. Testing new flame retardant materials on a milligram scale is cost efficient and can help engineer materials that prevent property and life loss to fires by inhibiting flame propagation.

Appendices

Appendix I-MATLAB Code Used to Process Calibration Images

```
%Black Body Calibrator
%(C)Fernando Raffan 2012

clear all
close all
clc

%First Run for D700 pictures
%Subscript 1 = red 650 nm
%Subscript 2 = blue (IR)900 nm

T = [900 950 1000 1050 1075 1100 1125 1150 1175 1200] ; %Calibration
temperatures
TK=T+273.15; %Convert T in C to Kelvin

%Calibration exposure times (shutter speeds)
redt=[1.6 1/1.3 1/2.5 1/4 1/5 1/8 1/10 1/15 1/20 1/25];
IRt=[1/3 1/6 1/10 1/13 1/15 1/25 1/25 1/30 1/40 1/50];

imagelistred=[6 7 8 9; 46 47 48 49; 50 51 52 53; 54 55 56 57; 58 59
60 61; 62 63 64 65; 66 67 68 69; 70 71 72 73; 74 75 76 77; 78 79 80
81];
imagelistIR=[5 6 7 8; 41 42 43 44; 45 46 47 48; 49 50 51 52; 53 54
55 56; 57 58 59 60; 61 62 63 64; 65 66 67 68; 69 70 71 72; 73 74 75
76];

%Calibration wavelengths
l1=650e-9;
l2=900e-9;

%Number of calibration images for each temperature
imnumber=4;

%Calibration coordinates (from prior visualization of image in
Matlab or
%Spotlight note x,y are swapped
pointR = [3649 2425];
pointIR= [3426 2425];

%Read Picture Files

for i = 1:length(T)
    for j= 1:imnumber

        if imagelistred(i)<10
   calib1 = imread([ 'RED_000' num2str(imagelistred(i,j))
'.tif'],'tiff');
        elseif imagelistred(i)<100
```

```
   calib1 = imread([ 'RED_00' num2str(imagelistred(i,j))
'.tif'],'tiff');
        elseif imagelistred(i)<1000
   calib1 = imread([ 'RED_0' num2str(imagelistred(i,j))
'.tif'],'tiff');
        else
        end

   data1=calib1(pointR(1),pointR(2),:);
   grayscale1(j)=mean(data1);

        if imagelistIR(i)<10
   calib2 = imread([ 'IFR_000' num2str(imagelistIR(i,j))
'.tif'],'tiff');
        elseif imagelistIR(i)<100
   calib2 = imread([ 'IFR_00' num2str(imagelistIR(i,j))
'.tif'],'tiff');
        elseif imagelistIR(i)<1000
   calib2 = imread([ 'IFR_0' num2str(imagelistIR(i,j))
'.tif'],'tiff');
        else
        end

   data2=calib2(pointIR(1),pointIR(2),:);
   grayscale2(j)=mean(data2);
    end

    GSred(i)=mean(grayscale1);
    GSIR(i)=mean(grayscale2);

    gstred(i)=mean(grayscale1)/redt(i);
    gstIR(i)=mean(grayscale2)/IRt(i);
end

figure
plot(T,gstred);
figure
plot(T,gstIR);

%Lumped Constant retrieval
h=6.626068e-34;
c=3e8;
kb=1.3806503e-23;
gstratio=gstred./gstblue;
A=h*c/kb;
B=(1/l2)-(1/l1);
C=exp(A*B./TK);
C2=exp(A*B/1700);
C2C1=C./gstratio; %Calibration constant; retrieve 1 per temperature

figure
plot(T,C2C1);
```

Appendix II-MATLAB Code Used to Determine Polymer Flame Angles

```
clear all
close all
clc

path='F:\Lab Work 2014\ALL (PS PSBr C3H8) 6-24-2014\POLYSTYRENE\650
Pics\';

pics=[17
18
23
24
25
31
32
33
34
35
37
45
46
47
48
49
]; %Number of pictures to test for symmetry. This can be the
starting and final number in a picture sequence
xsym=3671; %x location of assumed center of symmetry (burner center
location)
% yheights=3108;%y-location of 2 profiles of interest
ybase=3655; %burner base pixel location
profilewidth=100; %width of profile of interest. This can be
determined from examination of original image.


yheights=[2809
2819
2819
2863
2856
2857
2875
2817
2846
2869
2893
2812
2885
2837
2842
2876
]; % y pixel locations where line profiles are taken (0.7H)

yheights=yheights';

for i=1:length(pics)
```

```
    if pics(i)<10
    A=imread([path 'RED_000' num2str(pics(i)) '.tif'],'tiff'); %read
image file
    elseif pics(i)<100
    A=imread([path 'RED_00' num2str(pics(i)) '.tif'],'tiff');
    else
    end

    A=double(A); %convert to double precision for aritmentic
operations
    Amean=mean(A,3); %average to get grayscale
    profile1=Amean(yheights(i),1:xsym);%extract a profile that is +-
profilewidth pixels from assumed centerline
    xmax1=find(profile1==max(profile1));

    profile2=Amean(yheights(i),(xsym+1):7000);
    xmax2=find(profile2==max(profile2));
    realxmax2=xmax2+xsym;

    xcenterline=(xmax1+realxmax2)/2; % same process when determining
flame angle in propane flames, but x-pixel location of the max
intensity value on the line profile is used as "xcenterline"

    dy=abs(yheights(i)-ybase);
    dx=abs(xsym-xcenterline);

theta(i)=atand(dy/dx); %theta of how "off" you are wrt burner in
degrees
    end
```

Appendix III-MATLAB Code Used to Determine Flame Image Heights and Optimal Range of Flame Heights

```
% code for reading flame height (in pixels) for each test image

close all
clear all
clc

pics=5:1:55;
ybase=3725; % base of burner [pixel]
xsym=3723;  % burner centerline location [pixel]
pix2mm=85.5511811;

path='F:\Lab Work 2014\ALL (PS PSBr and C3H8) 5-13ish\650 pics
(C3H8)\'; % folder location where images are saved
color='RED';


for i=1:length(pics)
    if pics(i)<10
    A=imread([path color '_000' num2str(pics(i)) '.tif'],'tiff');
%read image file
    elseif pics(i)<100
     A=imread([path color '_00' num2str(pics(i)) '.tif'],'tiff');
%read image file
    else
    end

    A=double(A); %convert to double precision for aritmentic
operations
    Amean=mean(A,3); %average to get grayscale

%     frameinfo=double(read(obj,frames(i)));
%     frameinfoMean=mean(frameinfo,3);

    intensityline=Amean(:,xsym);

    intensitymax=max(intensityline);
    cutoff=0.10*intensitymax;    %used 10% as the cutoff for
propane; 20% for polymers

    locationcutoff=find(intensityline>cutoff);
    location(i)=ybase-min(locationcutoff);
    flameheight(i)=location(i)/(pix2mm);

end

%Scan Flameheight distributions
window=0.5; %Scan window in mm
average=mean(flameheight);
minheight=min(flameheight);
maxheight=max(flameheight);
%initialize scan loop
lowerlimit=minheight;
```

```
higherlimit=minheight+window;
counter=1;
step=0.33*window; %"step" size when shifting bin location

if higherlimit<maxheight

    while higherlimit<=maxheight
    [I,J,V]=find(flameheight<higherlimit & flameheight>lowerlimit);
    indices{counter}=J;
    bins(counter)=length(V);
    lowerlimit=lowerlimit+step;
higherlimit=higherlimit+step;
counter=counter+1;
counter

    end
else
    bins(i)=length(flameheight);
end
[blah,bestwindow,values]=find(bins==max(bins));
lowerlimit=minheight+step*(bestwindow-1);
higherlimit=lowerlimit+window;
bestimages=indices(bestwindow); %determine most populated bin of
image heights

figure
plot(flameheight,'o')
```

Appendix IV-MATLAB Code Used to Determine Flame Image Widths

```
clear all
close all
clc
pics=93:1:168;
xsym=3671; %x location of assumed center of symmetry (burner center
location)

yheights=[
2084
2080
2081
2069
2053
2062
2065
2059
2060
2063
2067
2080
2065
2070
2067
2060
2087
2126
2093
2070
2070
2051
2052
2065
2053
2070
2060
2065
2098
2081
2074
2085
2091
2095
2111
2093
2098
2039
2081
2087
2086
2093
2087
2088
2089
2081
2080
```

```
2086
2094
2093
2100
2098
2102
2101
2088
2076
2081
2104
2094
2094
2090
2080
2077
2086
2074
2087
2087
2073
2069
2078
2077
2074
2074
2033
2072
2089
];%y-pixel location of profiles of interest (0.7H)
ybase=3655; %burner base pixel location
profilewidth=500; %width of profile of interest. This can be
determined from examination of original image.

path='F:\Lab Work 2014\ALL (PS PSBr C3H8) 6-24-2014\C3H8\650 Pics\';

for i=1:length(pics)
    if pics(i)<100
    A=imread([path 'RED_00' num2str(pics(i)) '.tif'],'tiff'); %read
image file
    elseif pics(i)<1000
    A=imread([path 'RED_0' num2str(pics(i)) '.tif'],'tiff');
    else
    end

    A=double(A); %convert to double precision for aritmentic
operations
    Amean=mean(A,3); %average to get grayscale
    profile1=Amean(yheights(1),(xsym-
profilewidth):(xsym+profilewidth));%extract a profile that is +-
profilewidth pixels from assumed centerline
    xcenterline=find(profile1==max(profile1));
    profmax=max(profile1);
    profedge=0.02*profmax; %assigns edges of profile to cut off at
2% of the max value of the profile; in polymers determined using
"edge" function such that edges=edge(profile1);
```

```
    proffilt=profile1(profile1>profedge); %basically recreated new
profile with cut off edges
    proflengths(i)=length(proffilt);

end
```

Bibliography

Alaee, e. a. (2003). An overview of commercially used brominated flame retardants, their applications, their use patterns in different countries/regions and possible modes of release. *Environment International 29*, 683-689.

Alaee, M., & Wenning, R. J. (2002). The significance of brominated flame retardants in the environment: current understanding, issues and challenges. *Chemosphere*, 579-582.

Albemarle Corporation. (2011). *SAYTEX HP-3010 Flame Retardant.* Baton Rogue.

Ang, J. A., Pagni, P. J., Mataga, T. G., Margle, J. M., & Lyons, V. J. (1988). Temperature and Velocity Profiles in Sooting Free Convection Diffusion Flames. *AIAA Journal*, 323-329.

Babushok, V. e. (1998). *Chemical Limits to Flame Inhibition.* Gaithersburg: The Combustion Institute .

Birnbaum, L. S., & Staskal, D. F. (2004). Brominated flame retardants: cause for concern? *Environmental Health Perspectives*, 9-17.

Blue, C. e. (2000). High-Density-Infrared Transient Liquid Coatings. *The Member Journal of The Minerals, Metals & Materials Society*, 10-15.

Coffin, D. (n.d.). *Decoding raw digital photos in Linux.* http://www.cybercom.net/~dcoffin/dcraw/.

Collins, D. a. (1959). Two-dimensional convection from heated wires at low Reynolds numbers. *Journal of Fluid Mechanics, vol. 6*, 357-384.

Connelly, B. e. (2005). Two-dimensional soot pyrometry with a color digital camera. *Joint Meeting of the U.S. Sections of the Combustion Institute.* Philadelphia.

Darnerud, P. (2003). Toxic effects of brominated flame retardants in man and in wildlife. *Environment International*, 841-853.

Diez, F. e. (2009). Soot properties of laminar jet diffusion flames in microgravity. *Combustion and Flame*, 1514-1524.

Ding, X. (2013). *Design and Implementation of the Flaming Combustion Calorimeter.* College Park.

Fire Testing Technology. (2014). *Cone Calorimeter.* http://www.fire-testing.com/cone-calorimeter-dual.

Fu, T., Cheng, X., & Yang, Z. (2008). Theoretical evaluation of measurement uncertainties of two-color pyrometry applied to optical diagnostics. *Applied Optics*, 6112-6123.

Grause, G. e. (2013). Impact of brominated flame retardants on the thermal degradation of high-impact polystyrene. *Polymer Degredation and Stability*, 306-315.

Guo, H., Castillo, J. A., & Sunderland, P. B. (2013). Digital camera measurements of soot temperature and soot volumbe fraction in axisymmetric flames. *Applied Optics*, 8040-8047.

Huntsman, L.L.C. (2006). *Flammability and Toxicity of Expandable Polystyrene.*

Joo, H., & Gulder, O. (2009). Soot formation and temperature field structure in co-flow laminar methane-air diffusion flames at pressures from 10 to 60 atm. *Proceedings of the Combustion Institute*, (pp. 769-775).

Klimek, R., & Wright, T. (2004). *Spotlight-16 Image Analysis Software.*

Kuhn, P. e. (2011). Soot and thin-filament pyrometry using a color digital camera. *Proceedings of the Combustion Institute*, (pp. 743-750).

Linteris, G. (2011). *Advanced Gas-Phase Fire Retardants Project.* Gaithersburg: National Institute of Standards and Technology.

Lu, S.-Y., & Hamerton, I. (2002). Recent developments in the chemistry of halogen-free flame retardant polymers. *Progress in Polymer Science*, 1661-1712.

Lyon, R. E., & Walters, R. (2002). *A Microscale Combustion Calorimeter.* Egg Harbor Township: Federal Aviation Administration.

Lyon, R., & Janssens, M. (2005). *Polymer Flammability.* Springfield: National Technical Information Service.

Ma, B., & Long, M. B. (2012). Absolute light calibration using S-type thermocouples. *Proceedings of the Combustion Institute* (pp. 3531-3539). New Haven: Elsevier.

Mandatori, P., & Gulder, O. (2011). Soot formation in laminar ethane diffusion flames at pressures from 0.2 to 3.3 MPa. *Proceedings of the Combustion Institute*, (pp. 577-584).

Maun, J. D., Sunderland, P. B., & Urban, D. L. (2007). Thin-filament pyrometry with a digital still camera. *Applied Optics*, 483-488.

Mollmann, K. P. (2011). *Two-Color or Ratio Thermal Imaging-Potentials and Limits.* Germany: FLIR Systems.

Noto, T. e. (1996). Effect of Halogenated Flame Inhibitors on C1-C2 Organic Flames. *Twenth-Sixth Symposium (International) on Combustion* (pp. 1377-1383). Naples: National Institute of Standards and Technology .

Noto, T., Babushok, V., Hamins, A., & Tsang, W. (1998). *Inhibition Effectiveness of Halogenated Compounds.* Gaithersburg: The Combustion Institute.

Planck, M. (1901). On the Law of Distribution of Energy in the Normal Spectrum. *Annalen der Physik, vol. 4*, 553.

Sanders, e. a. (1989). *Bromination of polystyrene using bromine as the reaction solvent.* West Lafayette: United States Patent and Trademark Office.

Santoro, R. e. (1987). The transport and growth of soot particles in laminar diffusion flames. *Combustion Science and Technology*, 89-115.

Shaddix, C. R. (1999). Correcting thermocouple measurements for radiation loss: a critical review. *Proceedings of the 33rd National Heat Transfer Conference* . Albuquerque: American Society of Mechanical Engineering.

Shaddix, C. R. (2005). Flame structure of steady and pulsed sooting inverse jet diffusion flames. *Proceedings of the Combustion Institute*, 1501-1508.

SINTEF. (2005). *ISO 5660-1:1993: The Cone Calorimeter Test.* http://www.sintef.no/home/Building-and-Infrastructure/SINTEF-NBL-as/Key-projects-and-topics/Fire-testing-of-railway-seats/ISO-5660-11993-THE-CONE-CALORIMETER-TEST/.

Snelling, D. e. (2002). Spectrally resolved measurement of flame radiation to determine soot temperature and concentraion. *AIAA*, 1789-1795.

SpecialChem. (2014). *Electrical Engineering-LOI.* http://www.specialchem4polymers.com/tc/flame-retardants/index.aspx?id=9352.

Spengler, J. D., Allen, J. G., & McNeely, E. (2012). *Exposure to Flame Retardants in Commercial Aircraft.* Boston .

Sunderland, P., & Faeth, G. (1996). Soot formation in hydrocarbon/air laminar jet diffusion flames. *Combustion and Flame*, 132-146.

Sunderland, P., Koylu, U., & Faeth, G. (1995). Soot formation in weakly buoyant acetylene-fueled laminar jet diffustion flames burning in air. *Combustion and Flame*, 310-322.

Troitzch, J. (1990). *International plastics flammability handbook: principles, regulations, testing and approval* . Munich: Hanser Publishers .

Turns, S. R. (2012). *An Introduction to Combustion: Concepts and Applications.* New Delhi: McGraw Hill Education.

Underwriters Laboratories. (2014). *UL 94 Flame Rating.* http://www.ides.com/property_descriptions/UL94.asp.

Underwriters Laboratories. (2014). *UL94, the Standard for Safety of Flammability of Plastic Materials for Parts in Devices and Appliances testing.* http://www.ul.com/global/eng/pages/offerings/industries/chemicals/plastics/testing/flame/.

United States Environmental Protection Agency. (2014). *An Alternatives Assessment for the Flame Retardant Decabromodiphenyl Ether (DecaBDE).*

University of Central Lancashire. (2014). *Oxygen Index.* http://www.uclan.ac.uk/about_us/facilities/oxygen_index.php.

Urban, D. e. (1998). Structure and soot properties of non-buoyant ethylene/air laminar jet diffusion flames. *AIAA*, 1346-1360.

Weifang RuiDeSheng Chemical Co., Ltd. (2013). *Brominated Polystyrene Flame Retardant.* Shandong.

Yuan, Z.-G. (2003). *The Filtered Abel Transform and Its Application in Combustion Diagnostics.* Cleveland: NASA Center for AeroSpace Information.